

# Frequency of Hot Jupiters and Very Hot Jupiters from the OGLE-III Transit Surveys Toward the Galactic Bulge and Carina

Andrew Gould and Susan Dorsher

*Dept. of Astronomy, Ohio State University, 140 W. 18th Ave., Columbus, OH 43210, USA*

`gould,dorsher@astronomy.ohio-state.edu`

B. Scott Gaudi

*Harvard-Smithsonian Center for Astrophysics, 60 Garden Street, Cambridge, MA 02138, USA*

`sgaudi@cfa.harvard.edu`

and

Andrzej Udalski

*Obserwatorium Astronomiczne Uniwersytetu Warszawskiego, Aleje Ujazdowskie 4, 00-478 Warszawa, Poland*

`udalski@astrouw.edu.pl`

## ABSTRACT

We derive the frequencies of hot Jupiters (HJs) with 3–5 day periods and very hot Jupiters (VHJs) with 1–3 day periods by comparing the planets actually detected in the OGLE-III survey with those predicted by our models. The models are constructed following Gould & Morgan (2003) by populating the line of sight with stars drawn from the *Hipparcos* catalog. Using these, we demonstrate that the number of stars with sensitivity to HJs and VHJs is only 4–16% of those in the OGLE-III fields satisfying the spectroscopic-followup limit of  $V_{\max} < 17.5$ . Hence, the frequencies we derive are much higher than a naive estimate would indicate. We find that at 90% confidence the fraction of stars with planets in the two period ranges is  $(1/310)(1_{-0.59}^{+1.39})$  for HJs and  $(1/690)(1_{-0.54}^{+1.10})$  for VHJs. The HJ rate is statistically indistinguishable from that found in radial velocity (RV) studies. However, we note that magnitude-limited RV samples are heavily biased toward metal-rich (hence, planet-bearing) stars, while transit surveys are not, and therefore we expect that more sensitive transit surveys should find a deficit

of HJs as compared to RV surveys. The detection of 3 transiting VHJs, all with periods less than 2 days, is marginally consistent with the complete absence of such detections in RV surveys. The planets detected are consistent with being uniformly distributed between 1.00 and 1.25 Jovian radii, but there are too few in the sample to map this distribution in detail.

*Subject headings:* planetary systems – binaries: eclipsing – stars: radii

## 1. Introduction

More than 150 extrasolar planets have been detected to date, the majority by radial velocities (Butler et al. 2002; Mayor et al. 2004), but also by pulsar timing (Wolszczan & Frail 1992), microlensing (Bond et al. 2004; Udalski et al. 2005), and transits (Udalski et al. 2002a,b,d, 2003; Konacki et al. 2003a,b, 2004; Bouchy et al. 2004, 2005; Pont et al. 2004; Alonso et al. 2004). These planets and planetary systems exhibit a wide and unanticipated variety of characteristics, making the individual detections very interesting in themselves, to both scientists and the general public.

However, it is also important to derive from the ensemble of planet detections (and non-detections), the frequency of planets as functions of various parameters, such as mass, semi-major axis, and metallicity. This obviously requires a careful accounting of not only the catalog of detections, but also the stars for which planets would have been detected if they had had planets with various specified characteristics.

In deriving such rates from a given detection technique, the idiosyncrasies of that technique must be taken into account. Gaudi & Sackett (2000) developed a method for deriving rates for microlensing searches, which was first implemented by Gaudi et al. (2002) and later improved upon by others (Dong et al. 2005 and references therein). Rates have been derived from radial velocity (RV) detections by Nelson & Angel (1998), Cumming et al. (1999), and Cumming (2004), while Santos et al. (2005) and Fischer & Valenti (2005) have derived relative frequencies for RV planets as functions of planet and host properties. The detection efficiencies of various surveys for transiting planets in clusters have been calculated by Gilliland et al. (2000), Mochejska et al. (2005), Weldrake et al. (2005), and Burke et al. (2005).

The specific difficulty in deriving rates from transit surveys of field stars is that the luminosity and radius distributions of the target stars are not known (Gould & Morgan 2003; Brown 2003). This problem is made substantially worse by the fact that most transit surveys are directed toward fields in the Galactic plane where there is a huge background of high-

luminosity/large-radius sources, which dominate the star counts but whose planets would be almost completely undetectable. These difficulties are exacerbated by strong selection effects in field surveys such that the number of expected detections is a strong function of the planet and host star parameters (Pepper et al. 2003; Gaudi et al. 2005; Gaudi 2005).

These obstacles must be overcome if the full value of the field transit surveys is to be realized. The OGLE survey of Galactic-plane fields toward Baade’s Window and Carina raises many questions that are difficult to address in the absence of systematic rate studies. For example, why does OGLE detect VHJs even though RV surveys do not? Why does OGLE seem to detect so few HJs compared to RV? Why does OGLE detect comparable numbers of HJs and VHJs? Without a well-quantified rate study, it is impossible to determine if these apparent discrepancies are statistically significant and, if so, what is their physical origin.

The only studies to derive quantitative rate information from field transit surveys (Gaudi et al. 2005; Pont et al. 2005) avoided this problem by focusing on the question of relative frequencies of different classes of planets, rather than determining absolute frequencies. This enabled them to address some but not all of these questions. Moreover, using relative rates exacerbates uncertainties due to Poisson fluctuations. Hence, a more sophisticated treatment is needed.

Here we derive absolute frequencies of close-in planets from the OGLE transit survey. To determine the distributions of stars in the field as a function of luminosity and radius, we build on the work of Gould & Morgan (2003), who used the *Hipparcos* catalog to model local field populations. We generalize their approach to take account of possible variations in extinction and mean density along various lines of sight.

In §2, we review the OGLE-III transit data on which our analysis is based. In §3, we give a broad overview of how transiting planets are selected from the data and how these procedures are simulated in our models. In §4, we give a comprehensive summary of the selection procedures, and in §5 we give an in depth account of the most important aspects of modeling the resulting selection effects. In §6, we present our method for modeling the target populations of the OGLE-III survey, and in §7 we use our models to evaluate the number of stars actually probed for planets. This turns out to be far fewer than the number in the field satisfying the survey’s magnitude limit. In §8, we evaluate the frequency of planets derived from the OGLE-III survey and show that the rates are consistent those derived from RV surveys. §9 presents two Kolmogorov-Smirnov tests that demonstrate that the distributions of detections as functions of signal-to-noise ratio and *I*-band magnitude are consistent with the model predictions. §10 gives our prescription for incorporating the effects of limb darkening and ingress/egress. These effects, which we demonstrate to be only a few percent, are actually incorporated in the main analysis, but their description is deferred to

this section for clarity of presentation. In §11 and §12, we demonstrate that effects due to “resonances” near integer-day periods and due to unresolved binaries are small, of order a few percent. In §13, we investigate how well the scaling relations derived analytically by Pepper et al. (2003) for planet sensitivity as functions of planet radius and semimajor axis, apply to the OGLE-III sample. Finally in §14, we summarize our conclusions.

## 2. The OGLE Data

In 2001 and 2002, the OGLE-III project monitored approximately 155,000 disk stars for planetary transits. About 52,000 of these stars were in three fields toward the Galactic center, and the remaining 103,000 were in three fields toward Carina. The goal of the campaign was to test the utility of transits as a way to detect short-period planets. The campaign found both hot Jupiters (HJs), planets with periods between three and 10 days, whose analogs had previously been detected in RV surveys, and a new class of planets, the very hot Jupiters (VHJs), with still shorter periods.

The OGLE-III project observed three slightly overlapping fields toward the Galactic center between 12 June 2001 and the end of the Galactic bulge season in October 2001 using the 1.3-m Warsaw telescope at Las Campanas Observatory, Chile (operated by the Carnegie Institute of Washington), with a wide field CCD mosaic camera consisting of eight  $2048 \times 4096$  pixel SITe ST002A detectors. The bulk of the observations were made in 32 nights spanning the first 45 days, with single observations of each field taken every few days for the rest of the season. Altogether, about 800 images per field were taken in  $I$  with 120 second exposures. Additionally, several 150 second  $V$ -band exposures were taken to provide color information. However, the zero point of these  $V$ -band images is poorly calibrated (0.1 magnitude uncertainty). Because the star field is quite dense, no data were taken with seeing worse than  $1''.8$ . The median seeing was about  $1''.2$  (Udalski et al. 2002a).

Between February and May of 2002, the OGLE-III project observed three fields toward Carina in the Galactic disk ( $l \approx 290^\circ$ ) using the same telescope and camera as the bulge observations. Over the span of 95 days, about 1120  $I$ -band images per field were collected. Exposure times were 180 seconds and the median seeing was about  $1''$  (Udalski et al. 2002c).

OGLE observed an additional six fields in two additional campaigns during 2003 and 2004 (Udalski et al. 2004). These observations identified 40 additional planetary transit candidates. However, no RV measurements have been reported on these candidates, and thus it is not yet known which of these candidates have planets. We will not consider these two additional OGLE campaigns.

### 3. Philosophical Approach and Overview

As a practical matter, the sample is selected in three stages. First, OGLE identifies transit candidates derived from its photometric data. Second, all of these candidates are examined to identify those for which the transits can be ascribed to a cause other than a planet. Finally, the remaining candidates are observed spectroscopically to determine if they show RV variations consistent with a planet.

In order to extract planet frequencies from a comparison of the model with the planets detected by this procedure, it is essential that the procedure itself be well defined, *and* that the same selection criteria are applied to both the data and the model. This is by no means trivial because, as will become clear, the candidate sample was not selected by uniform criteria, nor even by a single group.

Our approach is to systematically review the selection procedures as reported in the literature and to identify uniform selection criteria that approximately represent these procedures. We then apply these same criteria to the model or, in cases for which this is impossible, take account of them by making statistical corrections to the model.

In order to guide the reader through this fairly involved exercise, we present in Table 1 a list of the various selection procedures, indicating in each case whether they were applied to the data and the model. In this section, we give a cursory summary of how each selection criterion was applied to the data and implemented in the modeling procedure. Substantially more detail is given for some of these criteria in the sections that follow.

**Construction of light curves.** We assume that the conversion of raw images to light curves is a transparent process that does not need to be modeled, except that saturated images are systematically removed. We identify this saturation limit empirically and impose it on the model. In particular, OGLE cleaned the data of systematics by comparing the behavior of each star with many neighbors, and we assume that this did nothing to corrupt the transit light curves.

**Automated OGLE Candidate Selection.** OGLE selected “pre-candidates” based on 6 criteria: transit depth  $\delta < 0.08$  mag, rms variability  $\sigma < 0.015$  mag, period  $P$  in the range 1.052–10.0 days, signal-to-noise parameter  $\alpha > 9$ , color-magnitude cuts (in the bulge fields only), signal detection efficiency  $SDE > \max[3, (4.9 - 0.1\alpha)]$ , and minimum number of transits (3 toward Carina and 2 toward the bulge). With the exception of the last two, all of these are straightforward to implement in the model. However, for three of these, we actually implemented stronger cuts on the model ( $\delta < 0.04$  mag,  $P < 5$  days,  $\alpha > 11$ ) and excluded any candidates not satisfying these more restrictive criteria from the data as well. Whenever a sample is cut a posteriori, i.e., after it has been searched for candidates, the

results can be biased toward higher detection rates. We discuss our reasons for making these more restrictive cuts in some detail and also argue that any bias is modest compared to the statistical errors. We assess the effect of the  $SDE$  cut by simulations and take this effect into account when reporting our derived rates. We also use simulations to measure the fraction of otherwise bona fide light curves that have insufficient transits to be selected by OGLE.

**By-eye OGLE Selection.** The above automated criteria yielded several thousand “pre-candidates” of which OGLE reported only 137 as “candidates”. The remainder were rejected by eye as being “spurious”. To model this procedure, one must determine the fraction of genuine transits that are eliminated in this by-eye step. We inject transits into real light curves to measure the fraction for which the transit search algorithm returns the wrong period. These would almost certainly be lost in the by-eye culling. For the remainder, we test directly that the same human (AU) who found the original transits can also find the injected transits that meet the objective selection criteria. Of course, if there were any planets transiting eclipsing-binary stars, the algorithm would return the binary’s period, and the light curve would be rejected as an eclipsing binary. We do not attempt to model this, but such systems are expected to be rare, in part because the eclipsing binary would often eject the planet.

**Feasibility of Followup.** For transit candidates to be confirmed as planets, their small velocity variations must be detected from high-resolution spectra. This will be impossible if the stars have very weak lines, either because they are spinning too fast or are of too early a type. As a practical matter, followup would be beyond the patience of the observers if the star were too faint. Of course, in a sample of transit candidates, one expects to find a fair number of stars that are spinning fast because they are tidally locked to a close-in massive companion. These are automatically eliminated from the data. However, we make no attempt to account for this in the model, since the fraction of fast-spinning late-type stars without massive companions is extremely small. We model the elimination of early-type stars by imposing a  $(V - I)_0 > 0.4$  cut in our simulation. We empirically determine  $V < 17.5$  as the effective limit beyond which observers “refused” to follow up candidates.

**Non-Eclipsing Binaries.** Our model assumes that all field stars are single, whereas more than half of G stars (which we demonstrate to be the primary target of the OGLE search) are known to be in binaries. We do not attempt to model this, but show analytically that the impact on our results is small.

## 4. Identification of Transiting Planets

### 4.1. Selection Criteria

We give a brief overview of the selection criteria and then give details on how they were applied.

1) The OGLE-III survey searched for detections down to a signal-to-noise-ratio ( $S/N$ ) parameter  $\alpha = 9$ , but based on the analysis reported in §5.3 we believe it is complete only to  $\alpha_{\min} = 11$ . In fact, the completeness is undoubtedly a rising function of  $\alpha$  rather than a strict step function, and our adopted threshold serves as a proxy for this continuous behavior. The lowest value for a planet actually detected by OGLE is  $\alpha = 11.8$ .

2) OGLE-III searched for periods in the range  $1.052 < (P/\text{day}) < 10$ . However, we further restrict the range to  $P < 5$  days. The primary reason for this is that, as summarized in §4.7, there was no systematic followup on 14 OGLE candidates with longer periods, so no useful scientific conclusions can be derived regarding planets with periods above 5 days. In addition, because such planets typically have very few transits, the modeling approach used in this paper would not yield accurate results on the survey’s sensitivity to them.

3) OGLE-III searched to a transit depth  $\delta < 0.08$  mag, but we further restrict this to 0.04 mag. Our primary reason for this is that, as summarized in §4.7, there was no systematic followup on 11 OGLE candidates with deeper transits. In principle, large planets (or small stars) might yield deeper transits, but if so they will be excluded from our sample. In practice, no planets have been discovered even near this boundary (despite the survey’s greater sensitivity to them) so this may be a real limit.

4) We require the source color to be  $(V - I)_0 < 0.4$  in order to eliminate early-F and A stars, which have few lines and so are inaccessible to RV followup.

5) We require  $V < V_{\max} = 17.5$  to account for the fact (discussed in §7.2) that the observers who carried out systematic RV followup observations were either unable or unwilling to monitor stars beyond this limit.

One must be careful when introducing a posteriori selection criteria: if planets had been discovered just past these boundaries, ( $\alpha < 11$ ,  $P > 5$  days,  $\delta > 0.08$  mag,  $(V - I)_0 < 0.4$ ,  $V > 17.5$ ) it is unlikely that they would have been excluded by hypothetical paper writers examining those data. However, regarding the period and depth criteria, we really do not have any choice because the data simply do not exist to conduct studies beyond our adopted limits. Regarding  $\alpha$ , we have done our best to impartially estimate this boundary. We also estimate that the error in our derived rates induced by an error in this boundary is of

order 10%, which is small compared to the statistical errors. The exact color boundary is difficult to estimate precisely, but there is little doubt that RV followup becomes impossible substantially beyond our adopted boundary. The  $V$  limit is the most difficult to properly estimate, but also has the least impact. The fact that a substantial number of stars were successfully monitored up to  $I \sim 16.4$  shows that the effective  $V$  limit cannot be too much brighter. On the other hand, in §7.3, we show that the OGLE-III survey does not have much sensitivity beyond this value anyway.

Of course, we eliminate all stars for which the transits can be shown to be due to binaries. We also eliminate stars with very weak spectral cross-correlation signatures regardless of their color. In principle, one would like to include these if they meet the other criteria. However, in practice, it is impossible to determine whether these stars have a planet or not. Moreover, given the prior that these stars have a short-period companion, the most likely explanation for their indistinct lines is that they are experiencing rapid rotation induced by tidal locking with a relatively massive companion.

We emphasize that these criteria are not adopted *ab initio*. Rather they are attempts to systematize the criteria that have been applied in practice by the workers who carried out the survey and followup observations.

## 4.2. Initial OGLE Selection

The OGLE-III bulge campaign initially identified 45 distinct sources that experience shallow-depth transits by cross correlating the observed light curve with artificial light curves of varying period containing a 0.015 magnitude transit of duration 0.03 times the period (Udalski et al. 2002a). After a reanalysis using a search algorithm developed by Kovács et al. (2002), 13 more candidates for planetary transits were found in the bulge. The Carina campaign initially identified 62 candidate sources using the same algorithm (Udalski et al. 2002c). An additional 6 bulge sources and 11 Carina sources surfaced after the correction for small scale systematic effects in both sets of data (Udalski et al. 2003). The objects selected by the Kovács et al. (2002) algorithm are characterized by two parameters  $\alpha$  and  $SDE$ .

In order to properly simulate the OGLE observations (and so derive planetary frequencies from them), it is essential to understand both of these parameters. The first parameter,  $\alpha$ , is closely related to but not exactly the same as the signal-to-noise ratio ( $S/N$ ). Whereas  $S/N$  is the ratio of the strength of the signal to the errors, which are determined from the *scatter around the best-fit transit curve*,  $\alpha$  is the ratio of the signal to the *scatter around a constant flux*. Since the scatter used to determine  $\alpha$  is inflated by the presence of the transit,



$\alpha$  is always strictly less than  $S/N$ . As we derive in §7.2,

$$\alpha = [(S/N)^{-2} + N_{\text{obs}}^{-1}]^{-1/2}, \quad (1)$$

where  $N_{\text{obs}}$  is the total number of observations. Thus, for  $N_{\text{obs}} = 1120$ , our adopted limit of  $\alpha_{\text{min}} = 11$  corresponds to  $(S/N)_{\text{min}} = 11.6$ , a relatively modest difference. However, the difference is accentuated at higher  $S/N$  because equation (1) implies that  $\alpha$  saturates at  $N_{\text{obs}}^{1/2}$ , i.e. at  $\alpha = 33$  in the present example.

The signal detection efficiency (*SDE*) is derived from the periodogram power spectrum. It is the ratio of the “peak excess” (peak minus the mean) to the standard deviation of this spectrum. OGLE eliminated candidates that failed to satisfy,

$$SDE > \max[3, (4.9 - 0.1\alpha)]. \quad (2)$$

Correlated errors inject power at many frequencies and thereby increase the dispersion of the power spectrum and so decrease the *SDE*. Since, as we show in §5.1, the OGLE errors are correlated, it will be crucial to determine how the *SDE* cut affects otherwise bona fide transit candidates.

### 4.3. Classes of Spurious Transit Candidates

Several different physical situations could have been responsible for the shallow transits seen by the OGLE survey. Some of these physical scenarios can be distinguished based on the OGLE observations alone, but others require additional spectroscopic and/or photometric data. Brown dwarfs, planets, and low-mass M stars all have about the same radius and are themselves dim. Thus, they produce comparable flux drops when they cross a star. Binary systems that are just barely eclipsing will create a shallow V-shaped dip in the light curve that may be picked up in a search for shallow transits. To further complicate matters, the blending of a faint (either dim or distant) binary system with another star can mimic a shallow transit. The faint binary system experiences a relatively large change compared to its own flux, but because this flux is itself small compared to the light added from the brighter nearby star, the fractional drop in the total flux is small and likely to be mistaken for a transit.

A variety of techniques can in principle distinguish these backgrounds from true planetary transits. V-shaped dips can be eliminated by visual inspection. Some bright-star/eclipsing-binary systems can be differentiated from planetary systems by measuring the light centroid shift during the eclipse. If the centroid does not shift, the system is most likely composed of a small companion (i.e., a planet, a brown dwarf, or a late M dwarf) transiting a star. For

an eclipsing binary system along the same line of sight as another star, the light centroid will most likely shift somewhat during the eclipse (Hoekstra et al. 2005).

#### 4.4. Culling Candidates Using OGLE Data

The single most effective technique for distinguishing false positives from transits is based solely on the OGLE data and eliminates about half the OGLE-III planetary transit candidates (Drake 2003; Sirko & Paczyński 2003). Stars with massive companions show variations in their light curves with a period equal to half the transit period. These variations are caused by the ellipsoidal shape of a star due to tidal distortion by its companion. For G0 stars, companions with a mass greater than about  $0.4M_{\odot}$  have ellipsoidal variability large enough that it can be distinguished from noise in the OGLE-III data, allowing these candidates to be eliminated without the need for followup measurements (Drake 2003). Even with these cuts, many cases remain for which additional photometric and spectroscopic observations are required to distinguish true planetary transits from various backgrounds.

#### 4.5. Photometric and Spectroscopic Followup

Three groups have used additional photometric data and low resolutions spectroscopy to further constrain the list of planetary transit candidates. Dreizler et al. (2002) observed 16 bulge candidates, including the 13 with the smallest companion radii as predicted by Udalski et al. (2002a), with the SAAO 1.9m telescope using the Grating Spectrograph. They obtained 1800s exposure,  $5 \text{ \AA}$  resolution spectra to classify the primary star in each system and thus obtain an estimate of its radius. Using this radius, coupled with the OGLE-III photometric data, they obtained an estimate of the companion’s radius in each system. They found two objects, OGLE-TR-03 and OGLE-TR-10 with radii of  $0.15R_{\odot}$ , which they believed were especially likely to be transiting planets. While extremely large radii are suggestive that a companion may not be a planet, the radii of short period planets are still poorly known. A spectroscopic followup campaign that selected against companions with large radii could easily miss detecting true planets.

Gallardo et al. (2005) combined the  $V$  and  $I$  band data from OGLE with their own  $K$  band data taken with the SOFI near-IR array at the 3.5m ESO New Technology Telescope. Exposure times were 3s per image, and the limiting magnitude was  $K \approx 17$ . Additionally, they took low resolution spectra with the Low Dispersion Spectrograph S2 (LDSS2) on the Magellan II 6.5m Clay telescope on 10 and 11 May 2003 using the  $1''$  wide slit with the high

resolution grating, yielding a  $6 \text{ \AA}$  resolution. Exposure times ranged from 90s to 600s. They estimated the effective temperature of the star in three different distance-dependent ways, such that a distance that makes the three temperature estimates consistent is likely to be the true distance of the star. One method used the correlation between dereddened color and effective temperature and the relation between reddening and distance to extract the effective temperature from the color. The second measurement was based upon the main sequence relation between mass and radius. The third measure (only possible for some stars) was directly from the low resolution spectrum. Stars with implausible distance solutions or inconsistent distance solutions are likely to be giants (OGLE-TR-83, 89, 98, 102, 116, 118, and 119). Once the distance is known, the absolute magnitude of the star can be calculated, and hence also its radius and the radius of its transiting companion. Gallardo et al. (2005) found OGLE-TR-105, 109, and 111 to be the most likely to host exoplanets because the radii of their transiting companions are less than  $0.14 R_{\odot}$ .

Heinze & Hinz (2005) obtained low-resolution spectra of OGLE-TR-134 through 137 on 12 and 13 June 2004, using the Boller & Chivens spectrograph on the University of Arizona 2.3 m Bok Telescope at Kitt Peak, in order to spectrally type these candidates. They were unable to definitively distinguish between giants and dwarfs, but on the conservative assumption that the stars were dwarfs, they estimated the stellar radius from the type and then estimated the planet radius from the transit depth. They found best-fit values and  $2\sigma$  errors (in units of Jovian radii,  $r_J$ ) of  $1.33 \pm 0.11$ ,  $1.43 \pm 0.12$ ,  $1.20 \pm 0.13$ , and  $1.63 \pm 0.16$  for the four candidates, respectively.

#### 4.6. Radial Velocity Followup

Following the RV confirmation of OGLE-TR-56 by Konacki et al. (2003a), which was the first discovery of a planet from transits, there have been two large campaigns to perform RV followup measurements of OGLE-III bulge candidates. Konacki et al. (2003b) obtained low resolution spectra for 39 of the 59 bulge candidates after eliminating 20 candidates based on secondary transits, V-shaped transits, or ellipsoidal variability in the light curves. Brighter stars were observed with the FAST spectrograph (R=4400) on the 1.5 m Tillinghast reflector at the Whipple Observatory on Mount Hopkins in May and June of 2002. The remainder were observed with the 6.5m Baade telescope Magellan I at Las Campanas Observatory using the Boller & Chivens spectrograph (R=2200) between 17 and 21 July 2002. These spectra allowed them to reject eight planetary transit candidates with early-type primary stars whose transiting companion must be large (and therefore stellar) in order to produce the observed drop in flux. Additionally, 25 low-depth grazing transits of stars could be rejected based

upon the relatively large RV variations (10 km/s) of these systems, which could be detected in the low resolution spectra. Six candidates remained following these rejections. Konacki et al. (2003b) obtained high resolution spectra for five of these six (OGLE-TR-3, 10, 33, 56, and 58) on the four nights between 24 and 27 July 2002 using the HIRES instrument ( $R=65000$ ) at the Keck I telescope. This group concluded that OGLE-TR-56 has a Jupiter-size companion, OGLE-TR-58 and OGLE-TR-10 either have planetary companions or are binary systems blended with brighter stars, and OGLE-TR-33 is a binary star system blended with a brighter star. While their own observations of OGLE-TR-3 were inconclusive, they reanalyzed the data of Dreizler et al. (2002) and concluded that it is probably a blended system. Konacki et al. (2005) later confirmed OGLE-TR-10 to be an exoplanet transiting its primary star. In brief, this campaign confirmed two OGLE-III candidates toward the Galactic bulge as transiting planets, OGLE-TR-56 (Konacki et al. 2003a) and OGLE-TR-10 (Konacki et al. 2005), while excluding many others.

Bouchy et al. (2005) performed independent RV followup observations of the OGLE-III bulge field planetary transit candidates. In October 2002 they observed three candidates (OGLE-TR-8, 10, and 12) with estimated companion radii less than  $1.6 r_J$  (as reported by Udalski et al. 2002a) using the UVES spectrograph on the ESO VLT, achieving a RV precision of  $54 \text{ m s}^{-1}$  on their best nights and a precision of  $93 \text{ m s}^{-1}$  overall. For each target, they made 8 measurements with exposure times from 20 to 40 minutes. Between May and June of 2003, they observed 17 candidates (OGLE-TR-5, 6, 7, 10, 12, 17, 18, 19, 33, 34, 35, 48, 49, 55, 56, 58, and 59) with the FLAMES multi-fiber link to the UVES spectrograph on the VLT, achieving a precision of about  $30 \text{ m s}^{-1}$ . These targets were selected to include the seven candidates with the smallest estimated radii according to Udalski et al. (2002a) plus a selection of candidates chosen to constrain the mass-radius relation of low mass stars. Bouchy et al. (2005) detected one transiting planet (OGLE-TR-56), one potential transiting planet that could also be a blended system (OGLE-TR-10), eight systems with stellar transiting companions (OGLE-TR-5, 6, 7, 12, 17, 18, 34, and 55), two grazing eclipsing binaries (OGLE-TR-8 and 35), two triple systems (OGLE-TR-33 and 59), one false positive (OGLE-TR-58), and three systems that could not be classified based on their observations (OGLE-TR-19, 48, and 49).

Pont et al. (2005) performed RV followup measurements for 42 candidates in the Carina field using the FLAMES facility with the UVES spectrograph on the VLT during eight half-nights 13 to 21 March 2004. This campaign yielded three confirmations of OGLE-III candidates as transiting planets, OGLE-TR-113 and OGLE-TR-132 (Bouchy et al. 2004) and OGLE-TR-111 (Pont et al. 2004). Targets were selected from the 73 OGLE transit candidates in Carina using indications found in the light curves, such as transit shape, radius of the eclipsing body, ellipsoidal variability, and/or secondary eclipses, to reject 43 candidates

that were almost certainly binaries. The remaining 30 candidates were ranked as first or second priority. All 14 first priority candidates were observed and 11 of the 16 second priority candidates were observed (OGLE-TR-70, 71, 73, 74, and 115 were not observed). The RV data reveal nine candidates with small stellar companions, one grazing eclipsing binary, four triple systems, one quadruple system, and fourteen systems that appear to be binaries but whose precise orbits were not determined. Two additional objects (OGLE-TR-124 and OGLE-TR-131) showed no RV variations in phase with the transit period ( $P < 2$  days in both cases) despite 8 RV measurements each with typical errors of  $\sim 60 \text{ m s}^{-1}$ . If they have VHJs, therefore, these must be less massive than  $0.3 M_J$  at the  $2\sigma$  level. A third object, OGLE-TR-109, showed large rotational broadening with correspondingly high RV uncertainties and no variation within those uncertainties. However, it seems to have the spectral temperature of an F-star, which makes the primary too large to host a HJ or a VHJ as a secondary given the transit depth. Seven more candidates possess no spectral lines strong enough for RV measurements. However, Pont et al. (2005) show that all but one object (OGLE-TR-82) cannot be isolated, slowly rotating late-type stars and thus they probably do not host a planet. The spectrum of OGLE-TR-82 had very little cross-correlation signal.

#### 4.7. Summary of Candidates

A careful accounting shows that, after imposing all of the selection criteria presented in §4.1, almost all of the OGLE-III planetary transit candidates have been either confirmed as planets or rejected.

Five of the candidates have proven to be planets transiting their primary star with a period between 1 and 5 days. These systems are summarized in Table 2. The vast majority of the remaining candidates are known to be binary star systems. Of those whose nature remains unknown, two have no lines useful for RV followup measurements (OGLE-TR-68 and 127), three have unknown periods (OGLE-TR-43, 44, and 46), and 14 have periods longer than 5 days and thus do not have a VHJ or a HJ in the period range relevant to the present study. An additional 11 systems have transit depths greater than 0.04 magnitudes, while all detected planets have transit depths less than 0.03 magnitudes and a typical value is more like 0.01 to 0.02 magnitudes. If any of these 11 candidates contain a planet, its nature must be substantially different from the 5 detected.

At this point, 4 systems of unknown nature remain: OGLE-TR-51, 82, 134, and 137. The properties of these systems are summarized in Table 3. OGLE-TR-51 is quite faint,  $I = 16.7$ . From OGLE-II photometry, we find  $V - I = 1.4$ . Hence,  $V = 18.1$ , well above our  $V_{\text{max}} = 17.5$  limit.

Pont et al. (2005) observed OGLE-TR-82, but the spectrum was too noisy to determine its nature. The 2MASS catalog indicates that this source is very red ( $I - J = 2.8$ ,  $J - H = 1.4$ , based on the OGLE  $I$  band magnitude and the 2MASS  $J$  and  $H$  band magnitudes). This red IR-based color is confirmed by a crudely calibrated OGLE-III optical color  $V - I = 3.3 \pm 0.2$ . Since  $I = 16.30$ , this implies  $V = 19.6 \pm 0.2$ , which is well beyond our limit and easily explains the difficulties that Pont et al. (2005) encountered obtaining a spectrum.

Heinze & Hinz (2005) “rule out” OGLE-TR-137 because they derive a large radius for the companion,  $r = 0.167 \pm 0.16 r_J$  ( $2\sigma$ ). This is a reasonable argument if all undiscovered planets have radii like those that have been found in the past. However, given the still exploratory nature of this field, one should adopt a more cautious attitude.

OGLE-TR-134 displays marginal evidence for ellipsoidal variations which, if confirmed, would indicate that the transiting companion was a low mass star rather than a planet. However, no firm conclusion can be drawn at present.

Until these two candidates are more thoroughly investigated, their status remains open. We handle the uncertainties about OGLE-TR-137 by restricting our inferences about planets to those with radii  $r < 1.5 r_J$ .

If OGLE-TR-134 turns out to have a planet, the rates derived in this paper will have to be revised upward. However, this will be straightforward given the tables that we provide.

## 5. Selection Effects

In our simulations, we will assume that genuine transit light curves with  $\alpha > 11$  are selected. However, this assumption could in principle fail for either of two reasons: the light curve failed the *SDE* cut and therefore was never examined by a human or it passed all cuts but was incorrectly rejected by humans. The false rejections can take one of two forms. First, the algorithm could return the wrong period, leaving the human to examine an incorrectly folded (hence garbled) light curve. Second, the light curve might be too noisy for reliable by-eye interpretation. In total then, there are three potential problems, which we examine in turn.

### 5.1. Correlated Errors: Effect of SDE Cut

As discussed by Pont et al. (2005), OGLE errors are correlated, which tends to drive down the *SDE*. Figure 1 shows the autocorrelation function for one of the 24 subfields in

Carina. That is, for each lag time  $\delta t$ , we measure the correlation coefficient of all pairs of measurements of the same star that are separated by  $\delta t$ . For the stars with the smallest errors ( $\sigma < 0.005$ ), the autocorrelation is extremely high (0.4) at the shortest time lag of 10 minutes and drops to 0.16 at 1 hour. While the autocorrelation is smaller for the more typical stars with larger errors, it does not approach zero until lag times of 2–3 days. Autocorrelation on the timescales of a transit (typically several hours) decreases the *SDE*.

To test the importance of this effect, we inject transits into the actual light curves of stars in the same Carina field by subtracting flux from the observations when a simulated planet passes in front of the star. We then analyze the resulting light curve using the same (Kovács et al. 2002) computer algorithm that OGLE used to find transiting planets. We consider 3 different periods ( $P = 1.123, 3.234, 4.86$  days), and three different depths ( $\delta = 0.008, 0.013, 0.024$ ). The planet phase and orbital inclination are drawn randomly. The duration of the transit is determined by assuming that the source is of solar mass and radius. We remove all light curves for which the correct period is not recovered to within 1% because this problem is evaluated separately in §5.2. Figure 2 plots *SDE* against  $\alpha$ . The points are color coded by the number of transits observed, ranging from magenta to red for 2 to 7 transits, with black representing light curves with 8 or more transits. As in the original OGLE-III analysis, 3 measurements must be made during a transit for it to count as a separate transit. Note that there are extremely few points with  $\alpha > 11$  and *SDE* below the threshold, while there would be many more such points were we to have adopted  $\alpha > 9$ . Note also that the bluer colored points (fewer transits) tend to have lower *SDE* at fixed  $\alpha$ , a trend that is expected for correlated observational errors. Finally, note that  $\alpha$  saturates at  $\alpha = \sqrt{N_{\text{obs}}} \sim 33$ , as expected from equation (1).

While very few transits are lost to the *SDE* cut, Figure 2 reveals another problem: there are a fair number of light curves with only 2 transits (magenta points), particularly at longer periods. OGLE-III eliminated these from its Carina sample, so we remove them from the model as well. Based on the diagrams in Figure 2 as well as others not shown, we find that the *SDE* cut and 3-transit cut together eliminate 0.5%, 1%, 2%, and 4% of genuine transits for period intervals of 1–2 days, 2–3 days, 3–4 days, and 4–5 days, respectively.

Figure 3 is a similar diagram for a bulge subfield. In this case, there are some points that fall below the *SDE* selection threshold. On the other hand, toward the bulge OGLE-III required only 2 transits (as opposed to 3 toward Carina). There are extremely few single-transit light curves that survive the period-recovery requirement. Toward the bulge we find that these two cuts eliminate 0.5%, 2%, 4%, and 9% for the 4 respective period intervals. We will take account of these casualties when we evaluate planet frequencies in §8.

## 5.2. Recovery of Transit Period

Several thousand light curves (the great majority toward Carina) passed the  $\alpha$  and  $SDE$  selection criteria, and OGLE examined each of these by eye to determine whether the transit was real. The great majority of these were obviously spurious, while a minority had to be studied more carefully to determine whether they displayed real transits. Since thousands of light curves had enough periodic power to be selected without any transits, one should ask whether the true period of any of the real transiting light curves was overwhelmed by a spurious period. If that occurred, then the folded light curve would have had the same characteristics as typical spurious transit light curves and most likely would have been rejected.

To address this question, we inject transits with five depths ( $\delta = 0.008, 0.010, 0.013, 0.018, 0.024$ ) into real light curves as described in §5.1, but with random periods between 1 and 5 days. We consider only light curves whose recovered parameters meet our  $\alpha$  and  $SDE$  selection criteria. We also demand that the “true” value of  $\alpha$  (based on the input parameters describing the transiting planet) be at least 9. We find that for virtually all the simulated light curves, the recovered period either agrees to well within 1% of the input period, or it disagrees by many percent. We set the threshold at 1% and ask what fraction of light curves have “bad periods” by this standard. We divide the sample into four period intervals, 1–2 days, 2–3 days, 3–4 days, and 4–5 days. Toward Carina we find that this fraction is roughly independent of depth and is about 6%, 10%, 13%, and 20%, in the four period intervals. Toward the bulge, the corresponding percentages are 2%, 9%, 15%, and 22%. We also take account of these losses when we evaluate planet frequencies in §8.

## 5.3. By-eye Selection

One of us (AU) did the original by-eye selection of the OGLE-III candidates and reported his subjective impression that this process was complete for  $\alpha > 12$ . To objectively test this impression, another member of our team constructed a sample of 61 light curves, 30 which contained artificial transits (injected into real light curves) with  $11 < \alpha < 13$  and periods of 3–5 days. This is the most difficult period range to vet because there tend to be fewer distinct transits, so the correlated noise shown in Figure 1 plays a bigger role. The remaining 31 light curves were taken from the original data. Both subsamples were selected from much larger ensembles of respectively simulated and real light curves, using the same algorithm to ensure that they displayed the broad range of distinct transits shown in Figure 2. AU then applied the same procedure to identify “true” transit candidates that he used to construct



the original sample. He identified 33 light curves as “real transits” and the remaining 28 as “spurious”. The first group contained all 30 simulated transits, plus 3 unmodified light curves from the original sample. All three of the latter had  $\alpha$  near the bottom of the investigated range,  $\alpha = 11.1, 11.2$  and  $11.4$ . Comparison with the list of original candidates showed that two of these had been identified in the original search (although one was subsequently removed because it has only 2 transits), while the third was not. Of course, it is not known whether this final light curve, which was missed in the original selection, is a real transit or not. However, it is not qualitatively different in appearance from others that are real.

The fact that 1 of 3 apparently real transits was missed in the original search while all 30 of the simulated transits were identified in the test indicates that the psychological conditions were probably more difficult in the former. This is plausible because a relative handful of real transits had to be culled from many thousands of spurious ones.

Based on these results, we estimate that the true effective threshold (i.e., the location of the step function that is the best proxy for the actual continuously declining completeness) is  $\alpha_{\min} = 11.0 \pm 0.5$ . In §8, we will evaluate the uncertainty in the final rates that is induced by this uncertainty in the true value of the threshold.

## 6. Modeling the Target Population

With the OGLE-III survey presumed complete for  $\alpha > 11$ , we are in a position to examine the statistics of HJs and VHJs. We would like to obtain the fraction of stars that have planets with any given mass and orbital period. For this, we need to know the number of systems that OGLE-III probed for planets of each period and mass. In an ideal world we would determine, for each star in the survey, which orbital periods and radii of planets would have been detectable had such planets been present at transiting inclinations. We could then assume that planets orbit at random inclinations relative to our line of sight and obtain the number of systems probed by the survey for any given kind of planet. The frequency of any type of planet is the number of similar planets detected divided by the number of systems probed for that kind of planet.

Unfortunately, this ideal approach is not possible because the distances to most stars in the OGLE-III survey are unknown. We cannot tell whether a given star is bright because it is close or because it is luminous. This degeneracy makes it impossible to determine whether a planet could have been detected around any specific star in the survey, since whether or not a planet is detectable depends on the star’s luminosity, radius, and distance. To circumvent this problem, we have created model star distributions for the OGLE-III Carina and bulge

fields based on the *Hipparcos* (ESA 1997) stars within 50 parsecs of the Sun and a simple Galactic model of stellar density. This model star distribution allows us to statistically determine the number of systems probed,  $N_p$ , for any kind of planet in the survey.

### 6.1. Star Distribution Model

The Galactic model we use has a double-exponential disk with scale height  $h = 250$  pc and scale length  $H = 2.7$  kpc, with the population at the Galactocentric distance  $R_0 = 8$  kpc fixed to fit observed local values. The characteristics of the star population (number density as a function of luminosity and radius) are derived from the *Hipparcos* catalog. Each *Hipparcos* star is given a weight equal to the inverse of the volume over which it could have been found.

*Hipparcos* is complete to visual magnitude  $V_{comp}(b) = 7.3 + 1.1 |\sin b|$ , where  $b$  is Galactic latitude. For stars  $M_V < 3.805$ , our sample consists of all stars with distances  $D < 50$  pc and hence the volume probed is  $\mathcal{V}_i = (4\pi/3)(50\text{pc})^3$ . For  $3.805 < M_V < 5$ , we consider stars with  $D < D_{7.3}$ , where  $D_{7.3}$  is the distance at which the star would have a magnitude of 7.3, hence  $\mathcal{V}_i = (4\pi/3)D_{7.3}^3$ . The selection is more complicated for the dimmest stars,  $M_V > 5$  for which we use  $D < D_{7.3+1.1|\sin b|}$ , i.e., the limiting latitude-dependent magnitude of *Hipparcos*, to define a non-spherical volume in which the star could be found.

$$\begin{aligned} \mathcal{V}_i &= \int_{-\pi/2}^{\pi/2} 2\pi d \sin b \int_0^{D_{7.3+1.1|\sin b|}} dD D^2 = \frac{4\pi}{3} \int_0^{\pi/2} d \sin b 10^{0.6(12.3-M_V+1.1 \sin b)} \\ &= \frac{4\pi}{3} \frac{e^\gamma - 1}{\gamma} 10^{0.6(12.3-M_V)} \text{pc}^3, \quad \gamma \equiv 0.6 * 1.1 * \ln 10. \end{aligned} \quad (3)$$

Each star is assigned an absolute magnitude  $M_V = V + 5 \log \pi - 10$ , where  $\pi$  is the measured *Hipparcos* parallax in mas and  $V$  is the *Hipparcos* input magnitude. It is also assigned a radius  $R_* = R_\odot 10^{0.597+0.536(B_T-V_T)-M_{V_T}/5}$  based on the prescription of Gould & Morgan (2003), where  $B_T$  and  $V_T$  are *Hipparcos* pass bands and  $M_{V_T}$  is the absolute magnitude in the  $V_T$  band.

For any given star,  $i$ , the expected number of identical stars between  $D$  and  $D + dD$  toward an OGLE-III field is given by

$$\frac{dN_i}{dD} = K \exp\left(-\frac{|z(D, b)|}{h}\right) \exp\left(\frac{R_0 - R(D, l)}{H}\right) \frac{\Omega D^2}{\mathcal{V}_i} \quad (4)$$

where  $(l, b)$  are the Galactic coordinates of the field,  $z(D, b)$  is the height above the plane at  $(D, b)$ ,  $R(D, l)$  is the Galactocentric distance at  $(D, l)$ ,  $K$  is a normalization constant to be

described below,  $\Omega$  is the solid angle covered by that field, and  $1/\mathcal{V}_i$  is the weight assigned to star  $i$  that characterizes its number density. The total number density of systems probed for planets in a given field is found by summing  $dN_i/dD$  over all the stars in our *Hipparcos* sample.

An extinction model based on a double exponential Galactic dust disk allows us to connect the three dimensional stellar density model to the two dimensional fields observed on the sky. We fix the dust scale length at the scale length of the stellar Galactic disk, but we fit for the dust disk scale height,  $h_{\text{dust}}$ . The local  $I$ -band extinction per unit distance,  $(dA_I/dD)_0$ , sets the normalization of this disk. The ratio of selective to total extinction,  $R_{VI}$ , is a fit parameter and is assumed to be constant along the line of sight. The following equation encapsulates our extinction model:

$$\frac{dA_I}{dD} = \left(\frac{dA_I}{dD}\right)_0 \exp\left(-\frac{|z(D, b)|}{h_{\text{dust}}}\right) \exp\left(-\frac{R_0 - R(D, l)}{H}\right). \quad (5)$$

The  $I$ -band extinction,  $A_I$ , to a given distance  $D$  is then given simply by the integral of this equation. The  $V$ -band extinction is  $A_V = A_I R_{VI}/(R_{VI} - 1)$ .

To fix the model star density empirically in each OGLE-III field, we produce a model binned color-magnitude diagram (CMD) and vary four parameters to maximize the likelihood of obtaining the observed OGLE-II CMD that lies along the OGLE-III field. We use OGLE-II data because they have calibrated  $V$  and  $I$  photometry. To produce the model CMD, we evaluate the color and magnitude at each distance (including extinction) and add  $dN_i(D, l, b)$  to the appropriate color-magnitude bin for each star. The four parameters varied are  $h_{\text{dust}}$ ,  $(dA_I/dD)_0$ ,  $R_{VI}$ , and  $K$ , which is a factor that normalizes the star density relative to the *Hipparcos*-based value.

We restrict the fit to the main sequence rather than the whole CMD because we only expect planets to be detectable around main sequence stars: giants have too large a radius, and the resulting magnitude change in transit would be too small to be detectable. To implement this restriction, we make the cuts shown in Figure 4 for the Carina field and in Figure 5 for the bulge field.

## 6.2. Resulting Fit Parameters

The top panels of Figure 6 show the OGLE-II color-magnitude diagram (CMD) for the Carina field and the best-fit model CMD, each binned by both color and magnitude. The whole observed OGLE Carina CMD is shown on the left, while the predicted CMD on the right shows only the region that was used to fit the model to the OGLE data. The lower

panels are the corresponding CMDs for the bulge fields. While the model CMDs reproduce the grossest OGLE CMD characteristics in both fields, the models and the observations are quite different in detail. This difference indicates that our model is too simple. *Hipparcos* stars may not be representative of OGLE stars. More likely, there are some density characteristics along each of the Carina and bulge lines of sight that are more complicated than a simple exponential disk. For instance, the Carina fields may pass through a spiral arm, while we neglect any such density fluctuations in our calculations.

To assess the impact of these discrepancies on our results, we evaluated the number of stars probed for planets for a variety of other models whose  $\chi^2$  lies within 20 of the minimum (at the best fit). We find that these differ by of order 10%, which is much less than the Poisson uncertainties arising from the small number of planet detections.

## 7. Number of Systems Probed

To establish the frequency of planets with a given radius and period, we compare the observed planets to the calculated number of systems probed for similar planets. To determine the latter, we must combine the *Hipparcos*-based model of the stellar distribution along the line of sight (§6) with the selection criteria by which the detected transiting planets were actually culled (§4). The most important of these is the signal-to-noise criterion,  $\alpha > 11$ , the modeling of which requires knowledge of the error distribution of the OGLE-III data set.

### 7.1. Error Functions

We estimate the photometric errors of the OGLE-III light curves from their scatter. Of course, this estimate is accurate only if the star is intrinsically stable: for variable stars the errors will be overestimated. However, for the relatively few non-transiting variables, the flux variations are a genuine source of noise that would interfere with the detection of a transit in a way that is very similar to photometric noise. This is because their more-or-less continuous variations have a very low correlation with the set of periodic, short-duration flux decrements that characterize the transit template used by the search algorithm. On the other hand, the number of transiting variables is so small that it has a negligible impact on the assessment of the photometric errors of the target population as a whole. Hence, the photometric scatter in this population is indeed the relevant quantity.

Our approach will be to estimate the photometric error as a function of *I*-band magnitude for each of the two target directions, Carina and the bulge. We must also check that a

single function reasonably describes all the subfields of each of these directions. We immediately confront the problem that the OGLE-III data are not precisely calibrated. Toward the bulge, each of the three fields overlaps a (calibrated) OGLE-II field, which enables a calibration accurate to a few hundredths of a magnitude. However, toward Carina, only one of the three fields overlaps OGLE-II. For the other two Carina fields, we obtain approximate calibrations by comparing OGLE-III flux levels to those of OGLE-III observations of OGLE-II fields made on the same photometric night. We expect these calibrations to be accurate to better than 0.1 mag.

We separately analyze a total of 48 subfields, 8 subfields for each of the three fields in each of the two target directions. For each we fit the errors,  $\sigma$ , to a cubic polynomial in the calibrated  $I$  magnitude. We eliminate the largest outlier and repeat the procedure until all  $2.5\sigma$  outliers are eliminated. The resulting 48 error functions (Fig. 7) are tightly clustered in two groups, one for each target direction. At the faint end, there is only one significant outlier (a Carina subfield), and that by a modest amount. While, there is some scatter in the error functions toward the bright end, the ensemble in each target direction can be reasonably represented as a single function.

We therefore repeat the above error-fitting procedure for an ensemble in each target direction. Because all three bulge fields are directly calibrated from OGLE-II data, we combine all 24 bulge subfields for this analysis. However, for Carina, we use only the 8 subfields of CAR100, the one Carina field that overlaps OGLE-II. In Figures 8 and 9, we show the resulting error functions together with the photometric scatter of each of the stars in the respective target directions. At faint magnitudes, the error functions closely track the peaks of the ridge lines in the data points. At bright magnitudes, they ride slightly above the ridge lines, but this properly reflects the asymmetric distribution of the data around the ridge line. Each figure also shows the  $2.5\sigma$  limits, beyond which all stars were removed from the analysis. In each case, about 10.3% of stars have been eliminated, the overwhelming majority because their errors are too large. To take account of this asymmetry, we will consider that these 10% of the stars contribute to planet detection with half the efficiency of the 90% that are well represented by the error function. This is obviously a crude approximation, but the error that it induces is more than an order of magnitude smaller than the Poisson errors, so a more exacting approach is not warranted.

The coefficients of the two cubics ( $\sigma = \sum_{k=0}^3 a_k I^k$ ) are

$$\begin{aligned} (a_0, a_1, a_2, a_3) &= (-0.72335462, 0.15435485, -0.01094052, 0.00025906) && \text{Carina} \\ (a_0, a_1, a_2, a_3) &= (-0.57434586, 0.12976481, -0.00973238, 0.00024385) && \text{bulge} \end{aligned} \quad (6)$$

We note that at faint magnitudes, the bulge fields have larger errors than the Carina

fields. This is partly because they have shorter exposures (120 vs. 180 seconds), and partly because the dense star fields toward the bulge add to the background “sky”. The two target directions are more similar at bright magnitudes, where the mean scatter falls to 0.005 and ultimately to 0.004 magnitudes in each case.

## 7.2. Maximum Distance for Planet Detection

The  $S/N$  of the transit in the light curve ultimately sets the maximum distance at which a planet could be detected around a given star ( $D_{\max}$ ). The depth of the transit and the photometric error determine the  $S/N$ :

$$S/N = \frac{\delta}{\sigma} \sqrt{\frac{N_{\text{tr}}}{N_{\text{obs}}}} (N_{\text{obs}} - N_{\text{tr}}), \quad (7)$$

where  $\sigma$  is the average photometric error in magnitudes associated with individual data points,  $N_{\text{tr}}$  is the number of data points in the light curve during transits,  $N_{\text{obs}}$  is the total number of data points in the light curve,  $\delta = (2.5/\ln 10)(r/R_*)^2$  is the fractional depth of the transit in the light curve,  $r$  is the radius of the planet, and  $R_*$  is the radius of the star. For a randomly sampled light curve,  $N_{\text{tr}} = fN_{\text{obs}}$ , where  $f$  is the fraction of the orbit spent in transit,

$$f = \frac{1}{\pi} \arcsin \sqrt{\frac{R_*^2 - b^2}{a^2 - b^2}}, \quad (8)$$

$a$  is the semi-major axis of the planet’s orbit, and  $b$  is the impact parameter of the planet on the star,  $0 < b < R_*$ . We address the potential complication of non-randomly sampled light curves in §11.

These equations implicitly assume that the transits are box-like, i.e., they ignore the light-curve distortions induced by limb darkening and ingress/egress. In fact, we take both of these effects into account. However, as we discuss in §10, the practical impact of these effects is small while the expressions representing them are cumbersome. Hence, for purposes of exposition, we initially ignore both effects.

As discussed in §4 and §5.3, we estimate that the survey is complete to  $\alpha_{\min} = 11$ . To incorporate this constraint into the simulation, we must relate the  $(S/N)$  to  $\alpha$ , which is defined analogously to equation (7) but with  $\sigma \rightarrow \sigma_{\text{scatter}}$ . Because  $\sigma_{\text{scatter}}$  is determined from the light curve *without* fitting for the transit, it is augmented relative to  $\sigma$  by

$$\sigma_{\text{scatter}}^2 = \sigma^2 + \frac{\delta^2 N_{\text{tr}} (N_{\text{obs}} - N_{\text{tr}})}{N_{\text{obs}}^2}. \quad (9)$$

Substituting this equation into equation (7) yields equation (1) for the relation between  $\alpha$  and  $(S/N)$ . Since there are approximately 1120 and 800 observations in the Carina and bulge fields, our adopted threshold of  $\alpha_{\min} = 11$  translates into

$$(S/N)_{\min}^{\text{Carina}} = 11.647, \quad (S/N)_{\min}^{\text{bulge}} = 11.940 \quad (10)$$

For each *Hipparcos* star, we invert equation (7) using  $S/N = (S/N)_{\min}$  to obtain the maximum photometric error at which a planet could be detected ( $\sigma_{\max}$ ). We then invert equation (6) to find the faintest  $I$  mag at which the transiting planet could be detected.

Next, we dim each star for dust  $I = I_0 + A_I(l, b, D)$  according to equation (5). This extinction as a function of distance, combined with the distance modulus and the absolute magnitude of the star, allows us to convert from the maximum magnitude at which a planet could be detected to the maximum distance at which that planet could be detected ( $D_{\max}$ ). We calculate the number of stars ( $N_S$ ) around which that planet could be detected if it transited the middle of the star ( $b = 0$ ):

$$N_S = \sum_i \int_{D_{\min,i}}^{D_{\max,i,b=0}} dD \frac{dN_i}{dD}, \quad (11)$$

where  $D_{\min,i}$  is the minimum distance to which star  $i$  can be detected, which is set by the saturation limits shown in Figures 8 and 9. The number of systems probed for planets ( $N_p$ ) by the OGLE-III survey is significantly less than  $N_S$  because planets orbit stars at a random inclination to our line of sight, rather than edge on. Naively, this would imply an additional multiplicative factor of  $R_{*,i}/a$ , where  $R_{*,i}$  is the radius of star  $i$  and  $a$  is the semi-major axis of the planet’s orbit, to account for the probability of a transit. In fact, because  $D_{\max,i}$  is a function of transit duration (and so of impact parameter), we must integrate over impact parameter from  $b = 0$  to  $b = R_{*,i}$  for each star:

$$N_p = \sum_i \int_0^{R_{*,i}} \frac{db}{a} \int_{D_{\min,i}}^{D_{\max,i,b}} dD \frac{dN_i}{dD}. \quad (12)$$

Udalski et al. (2002a,c) remove a number of light curves from their sample before running the transit search algorithm in order to eliminate unlikely candidates with minimal effort. We include these cuts in our calculations by modifying the maximum distance, instituting a minimum distance, and discarding stars as appropriate. In both the Carina and bulge fields, transit depths greater than 0.08 mag were discarded prior to running the transit detection algorithm. In our calculations, we discard transits with depths greater than 0.04 mag to match the set of OGLE-III candidates we consider. Additionally, Udalski et al. (2002a,c) reject light curves with rms variations greater than 0.015 mag in all fields. We exclude such stars from our model, taking account of both photometric errors and the additional scatter

induced by the transit itself. In the bulge fields, Udalski et al. (2002a) select light curves using a cut in the CMD in order to limit candidates to those on or near the main sequence. Our calculations account for this cut by introducing a minimum distance necessary to dim and redden the star to within the accepted region. As mentioned above, the saturation threshold in each field also imposes a minimum distance. We then integrate from the minimum distance to the maximum distance, rather than from zero to the maximum distance.

Photometric searches for planets by this technique are limited not only by transit detection, but also by the feasibility of RV followup measurements. RV measurements are limited by two factors: the  $V$ -band magnitude of the star (which influences the  $S/N$  of the spectrum) and the presence of spectral lines. In the analysis that follows, we will restrict our attention to stars with  $(V - I)_0 > 0.4$  in order to eliminate early-F and A stars, which have few spectral lines. The  $V$ -band magnitude limit for RV measurements combines with the intrinsic color limit and an average reddening to produce an apparent  $I$ -band magnitude limit. The distribution of observed  $I$ -band magnitudes of the candidates that proved susceptible to RV follow up suggests that RV detections of transit candidates are complete to an effective  $I_{\max} = 16.4$ . From this, we infer a true  $V$ -band limit by adding the  $V - I$  limit and an average reddening (derived from our simulations) of  $A_V = 0.7$  to obtain  $V_{\max} = 17.5$ . In our simulations, we implement these cuts by eliminating *Hipparcos* stars that are too blue ( $V - I < (V - I)_{\min}$ ) and by truncating our summation for each *Hipparcos* star at the distance at which the star reaches  $V_{\max}$ .

### 7.3. Number of “Good” Stars

It has been widely noted (Gould & Morgan 2003; Brown 2003; Pont et al. 2005; Gaudi et al. 2005) that there seem to be far too few planets detected in the OGLE-III survey based upon the planet frequency derived from RV surveys. The argument for this apparent inconsistency goes as follows: RV surveys found HJs orbiting roughly 1% of all stars. At the orbital radii under consideration, the geometric transit probability is about 10%. Since both the OGLE Carina and bulge fields contains several tens of thousands of stars up to the limiting magnitude for planet detection ( $V_{\max} = 17.5$ , see  $N_D$  in Table 4), one would naively expect about 40 planets to be detected in the Carina field and about 80 planets to be detected in the bulge field. In reality, 5 planets were detected between the two fields.

We partially solve this seeming paradox based on data from our simulations. We find that the OGLE-III transit survey is sensitive to planets for only a small fraction of stars in the field. The number of stars probed for planets at transiting inclinations,  $N_S$ , is given by equation (11), which indirectly depends on the limiting visual magnitude,  $V_{\max}$ . Table 4



shows  $N_S$  in both the Carina and bulge fields for several different  $V_{\max}$ . Table 4 also shows  $N_D$ , the approximate total number of stars in the field that are brighter than  $V_{\max}$ . Because the OGLE-III survey does not have secure  $V$  magnitudes, we scale the number of stars in a corresponding OGLE-II field by the ratio of the solid angles occupied by the OGLE-III and OGLE-II fields to obtain  $N_D$ . The ratio  $N_S/N_D$  shown in Table 4 gives the fraction of stars in the field that are actually probed for transits. If the above reasoning is applied to  $N_S$  rather than  $N_D$ , one should expect to detect 9 planets versus the 5 actually found, which is not such a big discrepancy. Actually, a proper comparison (given next in §8) must take account of the precise period and planet-radii intervals probed.

At our adopted  $V_{\max} = 17.5$ , only about 16% of the stars toward Carina and 4% of the stars toward the bulge can be probed for planets (of radius  $r = 1.2 r_J$  and semimajor axis  $a = 7.94 R_\odot$ ). These numbers are qualitatively similar to the 10% found by Gould & Morgan (2003) for transit surveys of bright ( $V_{\max} = 11$ ) stars.

Notice also that if the limiting followup magnitude were increased from  $V = 17.5$  to  $V = 18$ , the total number of systems probed would only increase by 16%.

Figure 10 shows the number of systems probed based on our stellar model for planets as a function of  $M_V$ ,  $(V - I)_0$  color, distance from the Galactic center  $R_{GC}$ , and star radius  $R_*$  for the Carina and bulge fields. These plots were produced by applying the technique outlined in §6.1 (together with the error function evaluated in §7.1) to the star-distribution model with the best-fit parameters to the observed CMD.

In both fields, the distribution of stars probed peaks at early G stars, as judged by either their color, absolute magnitude, or radius. The stars typically lie about 1 kpc from the Sun: toward the bulge, this places them at a Galactocentric distance of about 7 kpc, while toward Carina, their Galactocentric distance is more similar to that of the Sun.

## 8. Frequency of Planets

To make the most of sparse observational data dominated by Poisson noise, we bin the 5 detected planets in one-day-wide bins according to period. For example, for each period bin we calculate the average number of systems probed for the range of periods within that bin but for the full range of radii ( $1-1.25 r_J$ ). We convert the period of the planet to the semi-major axis (used in our computations) by assuming a stellar mass proportional to the radius for stars smaller than the Sun and by assuming solar mass for stars with larger radii. (To check the sensitivity of our results to this assumption, we have also performed the calculations assuming all stars are solar mass. The results agree to better than 10%.) See

Table 5. In constructing this table, we take account of the selection effects analyzed in §5. In particular, in each field we reduce  $N_p$  by the factors derived in §5.1 to account for transit light curves lost to the *SDE* and minimum-transit-number cuts and by the factors derived in §5.2 to account for the light curves whose periods are not accurately recovered by the search algorithm. Finally, we note that OGLE only searched for periods  $P > 1.052$  days, so we restrict our simulation to this range as well.

To establish the frequency of planets as a function of radius, we perform a similar calculation, this time binned by planet radius and integrated over the period range of 1–5 days. See Table 6. In Figure 11, we show the sensitivity to planets for each of the two fields, in each of two period ranges,  $1 \text{ day} < P < 3 \text{ days}$  and  $3 \text{ days} < P < 5 \text{ days}$ .

From Table 5, there were a total of 3 planets detected in the 1–3 day period range from among 2062 stars probed, and there are 2 planets detected from among 618 stars probed in the 3–5 day range (for planet radii uniformly distributed over  $1 < r/r_J < 1.25$ ). These detections yield rates of  $1/690$  and  $1/310$  respectively. Because of the small number of detections, the errors in these estimates are completely dominated by Poisson statistics. At 90% confidence we find that the frequency  $F$  in these two ranges is

$$\frac{1}{1640} < F[1 < P/\text{day} < 3] < \frac{1}{280} \quad (90\% \text{ C.L.}), \quad (13)$$

$$\frac{1}{650} < F[3 < P/\text{day} < 5] < \frac{1}{140} \quad (90\% \text{ C.L.}), \quad (14)$$

From Table 6, the distribution of planet radii is consistent with being flat between 1.00 and  $1.25 r_J$ . We have sensitivity to planets with larger radii, up to  $1.5 r_J$ , but do not find any. For all radii  $1.3 < r/r_J < 1.5$  we probe at least 1190 stars. Hence, at 95% confidence, we place an upper limit of  $F < 1/400$  for such large-radius planets in the period range of 1–5 days. (We use 95% one-sided limit here so that it can be directly compared to the upper limit in the two-sided 90% limits reported in eqs. [13] and [14].)

Our sensitivity to planets with  $r < r_J$  is much weaker. Nevertheless, we can place a 95% C.L. upper limit of  $F < 1/55$  for a model of planets uniformly distributed from 0.78 to 0.97 Jovian radii.

In §5.3, we estimated the completeness threshold and uncertainty to be  $\alpha_{\min} = 11.0 \pm 0.5$ . This corresponds to a fractional error of 4.5%. By repeating our analysis with  $\alpha_{\min} = 12$  rather than 11 (including estimating the reduced numbers of light curves lost to the *SDE* cut, bad period recovery, etc.) we find that the survey sensitivity scales as  $(S/N)^{-n}$  where  $n = 2.5$  for all period intervals and  $n$  ranges from 2.0 for  $r = 1.0 r_J$  to 3.0 for  $r = 1.25 r_J$ . Hence, the 4.5% uncertainty in the true threshold for  $\alpha$  translates into a  $2.5 \times 4.5\% \sim 11\%$  uncertainty in the sensitivity of the survey. This is small compared to our statistical errors.

### 8.1. Comparison with RV Detections

Are the rates reported here for HJs and VHJs consistent with the results from RV surveys? Two RV groups have presented data from which such a comparison can be made. We begin by examining the catalog of RV planets assembled on the California & Carnegie Planet Search website <http://exoplanets.org/almanacframe.html> (last updated 6 Feb 2005) and restrict this sample to planets that were detected in the survey of 1330 FGKM stars described by Marcy et al. (2005). There are 15 stars harboring planets with periods  $P < 5$  days: (HD73256, HD83443, HD46375, HD179949, HD187123b, HD120136, HD330075, HD88133, BD-103166, HD75289, HD209458, HD76700, HD217014, HD9826b, HD49674). From the lack of references to the California & Carnegie search team, three of these (HD73256, HD330075, and HD75289) do not appear to be part of their sample. One star (HD88133) appears to be part of a separate sample of metal-rich stars being surveyed by Fischer et al. (2005). This leaves 11 planets with periods in the range  $2.985 \leq (P/\text{day}) \leq 4.950$ . Even though one of these (HD83443) has a period that is slightly shorter than 3 days, it is fair to compare the entire group with the HJ transit sample. However, not all of these planets could have necessarily been detected by the OGLE-III transit survey. The four lowest-mass planets (HD49674, HD76700, HD46375, and HD83443) have masses  $M \sin i/M_J = 0.11, 0.19, 0.25,$  and  $0.41,$  respectively. In a sample of 11 planets with random inclinations, one expects one of these to have  $\sin i \sim [1 - (10/11)^2]^{1/2} = 0.42$ , so the appearance of HD83443 at  $M \sin i = 0.41 M_J$  would not be unusual even if all the planets in this sample were of roughly Jovian mass. However, the fact that 3 of the planets have  $M \sin i \leq 0.25 M_J$  indicates that they are probably genuinely of substantially lower mass. Thus, one may suspect that they are also of lower radius, but this is far from certain. On the one hand, in the solar system all gas giants have roughly the same density. If that rule applied here, these planets would be smaller by a factor 0.48 to 0.63. Inspection of Table 6 shows that the transit sensitivity drops off dramatically at these radii. On the other hand, both of the HJs found in the OGLE-III survey (OGLE-TR-10 and OGLE-TR-111) have radii  $r \sim r_J$  despite their low mass,  $M \sim 0.5 M_J$ . See Table 2. If this trend continued to still lower masses, then all 11 of the RV planets in the Marcy et al. (2005) survey would be accessible to the OGLE-III transit survey. To be conservative (in the sense of minimizing the apparent conflict between the planet frequencies as determined by the two methods), we adopt 8 as the number of the RV planets in the Marcy et al. (2005) survey of 1330 stars that could have been detected in the OGLE-III transit survey. However, for completeness, we also report below the results of a comparison based on that number being 11. Any of the 5 planets detected in the OGLE-III transit survey would have been detected by RV (had they been orbiting stars in the Marcy et al. 2005 sample) unless they were at improbably low inclination angles. Thus we should ask whether it is statistically plausible that  $(\text{planet-detections})/(\text{systems-probed})$  should be

2/618 for transits given that it is 8/1330 for RV, assuming that the underlying frequency,  $F$ , is the same for both samples.

Since it appears naively that there are too few transit detections, we formulate this question as: what is the probability that 2 or fewer planets were detected given that 618 $F$  were expected? We average over all  $F$  weighted by its Poisson probability as determined from RV and a uniform-log prior. We find,

$$p_{\text{HJ}} = \frac{\int d \ln F P(n_1|N_1F) \sum_{i=0}^{n_2} P(i|N_2F)}{\int d \ln F P(n_1|N_1F)} = \left( \frac{N_1}{N_1 + N_2} \right)^{n_1} \sum_{i=0}^{n_2} \frac{(n_1 + i - 1)!}{(n_1 - 1)!i!} \left( \frac{N_2}{N_1 + N_2} \right)^i = 34\%, \quad (15)$$

where  $n_1 = 8$ ,  $N_1 = 1330$ ,  $n_2 = 2$ ,  $N_2 = 618$ , and  $P(n, \tau) = \tau^n \exp(-\tau)/n!$ . This is certainly not low enough to demonstrate a conflict, but one should nevertheless raise the question: Is there any reason to believe that the transit and RV surveys sample different populations and, in particular, that the transit sample should have a lower frequency of planets?

RV field samples are heavily biased toward metal-rich stars. They are selected on  $B - V$  color and are essentially magnitude limited in  $V$ . At fixed  $B - V$  color,  $dM_V/d[\text{Fe}/\text{H}] \sim -1.3$ . Hence, stars that are more metal rich by  $\Delta[\text{Fe}/\text{H}] = 0.3$  are over-represented in the sample by a factor scaling as luminosity  $L^{3/2}$  or  $10^{0.4*1.5*1.3\Delta[\text{Fe}/\text{H}]} = 1.7$ . As metal-rich stars are overabundant in planets (Santos et al. 2004; Fischer & Valenti 2005), the mean frequency of planets in a magnitude-limited RV survey of field stars will be significantly higher than the frequency in the underlying field population.

Transit surveys also suffer from this bias, but at a level that is about an order of magnitude smaller. Transit surveys are also magnitude-limited and are also color selected, although the color for OGLE-III is  $V - I$  rather than  $B - V$ . However, (if we ignore extinction for the moment), the effective depth of a transit survey scales as  $L^{3/2}R^{-7/2}$  (Pepper et al. 2003) rather than  $L^{3/2}$ . At fixed  $V - I$  color (and hence fixed surface brightness  $S \propto LR^{-2}$ ), the depth therefore scales as  $L^{3/2}(L/S)^{-7/4} = L^{1/4}S^{7/4}$ . Moreover, at fixed  $V - I$ , the scaling of  $M_V$  with metallicity is not as steep,  $dM_V/d[\text{Fe}/\text{H}] \sim -1.0$ . Hence, for the above example of  $\Delta[\text{Fe}/\text{H}] = 0.3$ , the enhancement is only  $10^{0.4*0.25*1.0\Delta[\text{Fe}/\text{H}]} = 1.07$ . Moreover, this amplification is further diminished by the effects of extinction, which undercuts the  $L^{3/2}$  volume advantage of brighter sources.

Hence, while there is no statistical evidence for a lower frequency of transiting HJs compared to RV HJs, we expect that such a trend may emerge as the size of the sample increases.

If we assume that 11 (rather than 8) of the RV planets would have been large enough to be detected in the OGLE-III survey, then equation (15) yields 17% (rather than 34%).

This would be a more notable (though still not very significant) discrepancy, but we again emphasize that it is not clear that all 11 of the RV planets could have been detected.

We can also test whether the complete absence of RV planets with periods  $P < 2$  days is consistent with the three such planets detected in the OGLE-III transit survey. We again apply equation (15), but with  $n_1 = 3$ ,  $N_1 = 2062$ ,  $n_2 = 0$ , and  $N_2 = 1330$ , and find

$$p_{\text{VHJ}} = \left( \frac{N_1}{N_1 + N_2} \right)^{n_1} = 22\%. \quad (16)$$

Hence, the RV and transit surveys are marginally consistent with respect to VHJs.

The Geneva group searched 330 stars for planets using RV, among which they found 2 HJs (HD209458 and 51Peg) and no VHJs (Naef et al. 2005). Since the detections rates are very similar to those of California & Carnegie Survey, but the sample is about 4 times smaller, the results are even more consistent with the rates derived from transits.

The Geneva group has also undertaken a much larger study, called ‘‘CORALIE’’, which has surveyed 1600 stars and should have by this time detected all HJs and VHJs in this sample. However, to date they have reported only 5 detections with  $P < 5$  days: HD75289 ( $P = 3.51$  day,  $M \sin i = 0.42 M_J$ ), HD73256 ( $P = 2.55$  day,  $M \sin i = 1.85 M_J$ ), HD83443 ( $P = 2.99$  day,  $M \sin i = 0.38 M_J$ ), HD209458 ( $P = 3.52$  day,  $M \sin i = 0.70 M_J$ ) and HD63454 ( $P = 2.82$  day,  $M \sin i = 0.38 M_J$ ). See [http://obswww.unige.ch/~naef/who\\_discovered\\_that\\_planet.html](http://obswww.unige.ch/~naef/who_discovered_that_planet.html). If this is indeed the complete list of short-period detections, the result is inconsistent at the 95% confidence level with the 11 such planets found by the California & Carnegie Survey among 1330 stars (even assuming the two samples are disjoint). Given this inconsistency, and given the fact that the Geneva group has not yet commented on their apparent low rate of detection, it seems premature to compare this result with the rates presented here for transit detections.

## 9. Consistency Checks

The results on planet frequency just derived depend critically on the premise that the search for transiting planets was complete over the parameter intervals assumed. The three biggest worries in this regard are:

- 1) The survey might not be truly complete all the way down to our assumed threshold of  $\alpha_{\text{min}} = 11$ .
- 2) The sensitivity might be overestimated if the enhanced correlation at bright magnitudes (low errors) seen in Figure 1 degraded OGLE’s ability to recognize transits.
- 3) We may have misestimated the effective cutoff at faint magnitudes imposed by the diffi-

culty in obtaining spectroscopic followup observations.

We discuss these concerns and our reasons for adopting the various limits in question in §7.2. Nevertheless, it seems prudent to undertake additional tests. To this end, we conduct two Kolmogorov-Smirnov (KS) tests, one for the cumulative distribution of the planets with respect to  $S/N$  and the other with respect to  $I$ -band magnitude. These are shown in Figures 12 and 13, respectively.

If the survey were seriously incomplete at low  $S/N$ , we should expect a deficit of detections relative to the predictions shown at the right side of Figure 12. No such deficit is seen. If the errors were seriously underestimated at bright magnitudes, then we should see a deficit at the left side Figure 13, while if the cutoff at faint mags had been misestimated, then there should be an excess or deficit of detections at the right side. No such excesses or deficits are seen. Formally, the KS tests yield probabilities of  $P(d) = 0.50$  for  $d = 0.342$  and  $P(d) = 0.82$  for  $d = 0.257$ , respectively.

## 10. Limb Darkening and Ingress/Egress

Two effects cause transit profiles to deviate from the boxcar form with which they are modeled in the Kovács et al. (2002) (hereafter BLS) search algorithm: limb darkening and ingress/egress. Here we evaluate these two effects. We give our prescription for including them in the simulation, but also show analytically that their effects are relatively small.

We first consider limb darkening by itself. In the linear approximation, limb darkening is parameterized by a coefficient  $\Gamma$  and induces a surface-brightness profile (relative to uniform) of

$$S(x) = 1 - \Gamma \left( 1 - \frac{3}{2} \sqrt{1 - x^2} \right) \quad x \equiv \frac{\theta}{\theta_*}, \quad (17)$$

where  $\theta_*$  is the angular radius and  $\theta$  is the angular position on the surface of the star. Because BLS is fitting to a bimodal flux distribution, it will include all points that have greater than half the mean depth as part of the transit and will exclude all those with less than half the mean depth. Hence, if  $\Gamma < (1 + 3\pi/8)^{-1} \sim 0.46$ , it will find a transit length equal to the chord traced by the center of the planet while it remains inside the limb, i.e.,  $2(1 - \beta^2)^{1/2}\theta_*$  where  $\beta$  ( $0 \leq \beta \leq 1$ ) is the normalized impact parameter. And it will find a “depth”  $\delta$  equal to the mean depth during this time interval,

$$\frac{\delta(\beta)}{\delta_0} = \frac{\int_{-Q}^Q dy S(\sqrt{\beta^2 + y^2})}{2Q} = 1 - \Gamma \left( 1 - \frac{3\pi}{8} Q \right) \quad Q \equiv \sqrt{1 - \beta^2}, \quad (18)$$

where  $\delta_0$  is the depth for a uniform surface brightness.

For perfectly edge-on transits ( $\beta = 0$ ), the mean depth is fractionally higher by  $0.18\Gamma$ , while for grazing transits ( $\beta \sim 1$ ), it is fractionally lower by  $-\Gamma$ . Hence, edge-on eclipses can be probed over greater volumes and grazing transits over smaller volumes than would be the case for a uniform surface-brightness source. One may expect that these two effects would cancel out, and we show below that this is approximately the case.

However, before doing so we introduce ingress/egress effects. These decrease the flux decrement (relative to the point-planet approximation) when the center of the planet is near, but still inside, the limb of the star, and increase it when the planet center is just outside the limb. However, from the standpoint of BLS, all information about the latter effect is lost because the flux is closer to its non-transit level, so the flux decrement is not included by BLS in its boxcar-approximation “transit”. To a first approximation then, BLS still finds a transit length of  $2Q$ , but the mean decrement is reduced to

$$\frac{\delta(\beta)}{\delta_0} = 1 - \Gamma \left(1 - \frac{3\pi}{8} Q\right) - (1 - \Gamma) \frac{\epsilon}{Q^2}, \quad \epsilon \equiv \frac{2}{3\pi} \frac{r}{R_*}, \quad (19)$$

where  $r$  is the planet radius and  $R_*$  is the star radius. The various factors in the final term can be understood as follows. The ingress/egress affects only the limb, where the flux is already reduced by a factor  $(1 - \Gamma)$ . The length of the ingress and egress (restricted to the relevant time when the planet center is inside the limb) is  $2(r/R_*)/Q$ , hence its fractional length is  $(r/R_*)/Q^2$ . Finally, the mean fraction of the planet that is actually over the limb during these interval is  $2/3\pi$ . We use  $\delta(\beta)$  as given by equation (19) in our simulations rather than the uniform surface-brightness value,  $\delta_0$ . Since the stars probed by the OGLE-III survey are primarily solar-type stars, we use the solar limb-darkening value  $\Gamma_I = 0.368$ . (This corresponds to  $c = 3\Gamma/(\Gamma + 2) = 0.423$  in the usual limb-darkening formalism, in which  $S(x) \propto (1 - c[1 - (1 - x^2)^{1/2}])$ .)

In fact, during the time when the planet center is extremely near (but still inside) the limb, the flux will be closer to its non-transit than its mean-transit value, and BLS will assign such points to the non-transit part of the light curve, thus shortening the fit duration below  $2Q$  and increasing the mean decrement relative to equation (19). This will lead to very slightly lower  $\chi^2$  and so to very slightly higher  $\alpha$  than implied by equation (19). However, the effect is second order in  $\epsilon$ . As we show immediately below, the first order  $\epsilon$  effects are already quite small, so we ignore these second order effects in the interest of simplicity.

We find numerically that the net effect of including both limb darkening and ingress/egress reduces the sensitivity of the OGLE-III survey by 5%–2%, for periods from 1 to 5 days. However, it is also instructive to understand this result analytically.

Suppose that near the threshold of a survey, the number of systems probed scales as  $(S/N)^n$ . For example, in the uniform-stellar-density, above-sky photon-limited noise case

considered by Pepper et al. (2003),  $n = 3$ , while below sky this would be  $n = 3/2$ . Then the total number of systems probed (relative to ignoring limb darkening and ingress/egress) would be

$$\eta(\Gamma, \epsilon; n) = \frac{\int_0^1 d\beta [\sqrt{Q}\delta(\beta)/\delta_0]^n \Theta[\delta(\beta)]}{\int_0^1 d\beta Q^{n/2}}, \quad (20)$$

where  $\Theta$  is a step function. In Figure 14, we evaluate this numerically for a broad range  $n$  and for  $r/R_* = 0, 0.075, 0.1, 0.125,$  and  $0.15$ .

By comparing results of simulations with  $\alpha_{\min} = 11$  and  $12$ , we determine for the OGLE-III data set, that overall  $n \sim 2.5$ , and ranges from 2 to 3 depending on what subclass of periods or radii are examined. Hence, the intersections of the curves with the dashed vertical line in Figure 14 are the most representative of the role of limb darkening and ingress/egress in the present case.

Over the range of power laws shown in Figure 14, limb darkening by itself affects the rate at the level of a few percent, and is generally positive and gently rising in the neighborhood of  $n = 2.5$  (relevant for the OGLE-III survey). On the other hand, ingress/egress affects the rate negatively, also by a few percent. The net effect at  $n = 2.5$  is negative at the 2–4% level, in agreement with what we found by directly inserting limb darkening and ingress/egress into the simulations.

## 11. Periodic Observations

In the simulations reported in §6, we assumed that the observations were taken at random times and hence that the fraction of all observations that occur in transit is exactly equal to the fraction of the orbit that the planet is transiting the star. However, real ground-based observations are not randomly sampled, but rather can only be made at night. Depending on the phase of the transit relative to the night, planets with periods close to an integer number of days will be seen in transit with a frequency that may be either much larger or much smaller than the average value we have used. If the number of observations in transit is greater than average, then the transit  $S/N$  for a given stellar type and given distance is also greater than average. Hence, the transiting planet can be detected to a greater limiting distance. Conversely, if the number of observations in transit is below average, then transits of stars of a given type will be detectable to a smaller distance.

For observations at a fixed ratio of transit depth to photometric error (but averaged over planets in all orbital phases at the start of the observations), these divergent behaviors can lead to a net enhancement or a net degradation of the survey sensitivity to planets near



integer-day periods (Pont et al. 2005; Gaudi et al. 2005). However, for searches extending to a given S/N limit, the effect can only be an enhancement (assuming a uniform density of sources and that extinction is not extremely severe). Before presenting our quantitative results, we examine this qualitative difference.

At sufficiently small transit depths (relative to photometric error) and for non-special periods, there will normally be too few observations in transit to yield enough S/N for a detection. However, near integer-day periods (and for some phases), the number of transit observations will increase by enough to meet the S/N threshold. Hence, the sensitivity will show upward spikes at integer periods. Conversely, at large transit depth, there will normally be more than enough observations to meet the S/N threshold, but near integer-day periods and for adverse phase alignment, there will be a shortfall. Hence, there will be negative spikes. Since transits are easier to detect at short periods, these two effects imply that there will be negative spikes at short periods and positive spikes at long period. All these effects are shown in Figure 12 of Pont et al. (2005) and Figure 4 of Gaudi et al. (2005).

However, these effects combine in quite a different way when considering a survey to fixed limiting S/N. Whether one is close to or far from an integer period, the *mean number* of transits (averaged over all phases at the start of observations) is the same. Hence, near an integer-day period, some phases have an amplified number of in-transit observations at the expense of other phases. Since (in the absence of extinction and with photon-limited above-sky errors), the maximum distance scales very nearly as the square root of the number of in-transit observations, the volume gained by the favorable phases exceeds the volume lost by the unfavorable ones. Hence, there is always a net gain in sensitivity near integer-day periods.

To be more quantitative, we define the amplification factor  $F_{amp} = \bar{N}_p(P)/N_{p,random}(P)$  as the ratio of the phase-averaged number of systems probed in a model ground-based observation scenario,  $\bar{N}_p(P)$ , of a planet with a period  $P$  to the number of systems probed in a randomly sampled observation scenario,  $N_{p,random}(P)$ . We derive  $F_{amp}$  from scaling relations. Assuming a constant density of stars in space (neglecting Galactic structure),  $N_p$  is proportional to the volume of space within the maximum distance to which a transit could be detected,  $\mathcal{V} = d^3$  ( $N_p \propto d^3$ ). Neglecting extinction, the flux is proportional to  $d^{-2}$ , while the photometric error of an individual data point  $\sigma$  is proportional to  $(\text{flux})^{-1/2}$ . Combining these scaling relations with the definition of  $F_{amp}$  and equation (7) gives,

$$F_{amp} = \frac{1}{Pf(1-f)} \int_0^P \left[ \frac{N_{tr}(\phi, P, f)}{N_{obs}} \left( 1 - \frac{N_{tr}(\phi, P, f)}{N_{obs}} \right) \right]^{3/2} d\phi, \quad (21)$$

where  $\phi$  is the phase,  $f$  is the fraction of the orbit the planet spends in transit,  $N_{tr}(\phi, P, f)$  is the number of data points in transit, and  $N_{obs}$  is the total number of data points. We

calculate  $N_{\text{tr}}(\phi, P, f)$  using a program that assumes 24-hour days, six hour nights, ten minute observations, an 80-day observing campaign, and  $f = (1/30)(P/4 \text{ day})^{-2/3}$ . Figure 15 shows  $F_{\text{amp}}$  as a function of period.

Using the data shown in Figure 15, we find that the average  $F_{\text{amp}}$  for periods from 1.5 to 4.5 days is 1.027. Thus, the net effect of periods resonant with the observing cycle on the calculated number of systems probed is  $< 3\%$ . To assess the impact of resonances on the distribution of periods that are actually observed, we calculate the fraction of the total number of systems probed found in the integer peaks (second row of Table 7) as compared to the fraction expected without amplification based solely on the widths of the peaks (first row of Table 7). For purposes of this calculation, we consider a “peak” to extend over the region within the interval  $(n \pm 0.05)$  days where the local enhancement is at least 5%. We find that integer-day resonances are not substantially more likely to be detected than other periods in the period range explored here, which is consistent with the planets actually detected. Since the net effect of resonances is small and resonant periods are not much more likely to be observed than non-resonant periods, we neglect integer-day resonances in our calculations.

## 12. Unresolved Binaries

As illustrated in Figure 10, the OGLE-III target sample is dominated by G stars, roughly 2/3 of which are expected to have binary companions (Duquennoy & Mayor 1991). At their typical distances of 1 kpc (see Fig. 10), most of these binaries would be unresolved. We ignore this blending by binaries when modeling the search process. However, we argue here that this has only a very small impact on the implied sensitivity of the survey.

We first note that the underlying *Hipparcos* data, which are used to model the field sample, are affected by exactly the same phenomenon. The physical separation at which blending sets in for the *Hipparcos* sample is about a decade smaller than for the field sample because the former is about 20 times closer, while the *Hipparcos* resolution is somewhat worse than that of OGLE. However, since there are roughly equal numbers of binaries per decade over 7 decades of separation, this is a relatively small difference. Hence the merged binaries are automatically assigned the correct combined luminosity by our modeling procedure.

For simplicity, let us now consider the special case in which the two components of the binary have the same surface brightness. Let the two stars have flux fractions  $f$  and  $(1 - f)$ , and let us initially focus on a planet transiting the first component. Our model will assign a radius to the star that is too large by a factor  $f^{-1/2}$ . Consequently, it will overestimate the duration of the transits by the same factor. This will in turn lead to an overestimate of the

$S/N$  generated by the transits by a factor  $f^{-1/4}$ . At fixed semimajor axis, this error in the radius estimate will also cause us overestimate the probability of a transit by a factor  $f^{-1/2}$ . Of more direct interest is the error at fixed period. In this paper, we have considered two mass-radius relations  $M = R^m$ , where  $m = 1$  for stars dimmer than the Sun and  $m = 0$  for stars more luminous than the Sun. Using Kepler’s Third Law, our overestimate of the transit probability is therefore  $f^{-1/2+m/6}$ . Combining these factors, and assuming the sensitivity of the survey grows  $\propto (S/N)^{-n}$ , we find that the sensitivity of the binary to planets relative to our erroneous treatment of it as a single star is

$$F_{\text{bin}}(f) = f^{n/4+1/2-m/6} + (1 - f)^{n/4+1/2-m/6}. \quad (22)$$

This expression deviates maximally from unity at  $f = 1/2$  (i.e., equal-mass binaries), for which  $F_{\text{bin}}(1/2) = 2^{1/2+m/6-n/4}$ . For  $n = 2.5$ , which is the appropriate approximation for the current survey, we obtain  $F_{\text{bin}} = 0.92$  and  $1.03$  for  $m = 0$  and  $m = 1$ , respectively. Since the majority of binaries are relatively far from equal-mass (Duquennoy & Mayor 1991), the typical effects are smaller. Hence, ignoring source binarity has relatively little impact on the results.

### 13. Scaling Relations

Pepper et al. (2003) predict the scaling relations between the number of systems probed ( $N_p$ ) and both the semi-major axis of the planet’s orbit ( $a$ ) and the planet’s radius ( $r$ ),  $N_p \propto a^{-5/2}r^6$  (Pepper et al. 2003). The top panel of Figure 16 shows the number probed in the Carina field as a function of  $r$  for several different values of  $a$ , and the bottom panel shows  $N_p$  in Carina as a function of  $a$  for several values of  $r$ . The best-fit slopes (or power law indices) of the  $a$  scaling relation in the Carina field are shown in Table 8, and the best-fit slopes of the  $r$  scaling relation in the Carina field are shown in Table 9. The results of our simulation are in qualitative agreement with the predictions of Pepper et al. (2003), which were derived under the idealized assumptions of uniform density, photon-limited noise, and no extinction. However, note that the actual power-law indices can deviate from these ideal values by up to 25% over the ranges explored in Tables 8 and 9, so caution is warranted when applying these relations.

### 14. Conclusions

We have measured the frequency of HJs ( $3 \text{ days} < P < 5 \text{ days}$ ) and VHJs ( $1 \text{ day} < P < 3 \text{ days}$ ) by calculating the numbers of stars probed for planets in the OGLE-III Carina and

Galactic bulge transit fields, and comparing these to the 5 planets actually detected. At 90% confidence, we find that the HJ frequency is  $(1/310)(1_{-0.59}^{+1.39})$  and the VHJ frequency is  $(1/690)(1_{-0.54}^{+1.10})$ . The HJ rate is consistent with the results of RV studies, and the VHJ rate is marginally consistent with the complete lack of RV detections for  $P < 2$  days. Because RV surveys are heavily biased toward metal-rich stars, which are known to harbor substantially more planets than average, we expect them to yield a higher rate of planet detection. However, the statistics are too sparse yet to be sensitive to this anticipated effect.

We find that the number of stars probed (to the limit set by the followup threshold of  $V_{\max} < 17.5$ ) is less than number of stars in the field to this limit by roughly a factor 6 toward Carina and a factor 25 toward the bulge. The remainder of the stars have physical radii that are too large to permit a detectable transit signal. Hence, a careful determination of the number of *accessible* stars in a given field is required to produce reliable estimates of the planet frequency.

The five OGLE-III planets are consistent with being uniformly distributed between 1.00 and 1.25 Jovian radii, although the number of detections is too small to probe this distribution in detail. The survey has deteriorating sensitivity at smaller radii, but would have detected planets of larger radius, had a substantial such population been present. We place a 95% confidence upper limit of  $F < 1/400$  on planets with  $1.3 < r/r_J < 1.5$  in the period range of 1–5 days.

Additionally, we have investigated the impact of four effects on the sensitivity of the OGLE-III survey to planets with periods of 1–5 days and found this to be of order a few percent in each case. These include limb darkening, ingress/egress, the periodic nature of ground-based observations, and unresolved binaries. The first two were specifically included in our simulations while the latter two were not.

Finally, we have also shown that the scaling relations predicted by Pepper et al. (2003) are approximately valid for planets probed in the OGLE-III survey, but that the actual power-law indices can deviate from the predicted ones by up to 25% over the parameter ranges we explored.

We are grateful to Frédéric Pont, whose extensive comments, in several iterations, added greatly to our understanding of the selection effects operating in the OGLE survey. Work by AG and SD was supported by grant AST-0452758 from the NSF. Work by BSG was supported by a Menzel Fellowship from the Harvard College Observatory. A.U. was supported by the following grants: Polish MNII 2P03D02124, “Stypendium Profesorskie” of the Foundation for Polish Science, NSF AST-0204908 and NASA NAG5-12212. Any opinions, findings, and conclusions or recommendations expressed in this material are those of the

authors and do not necessarily reflect the views of the NSF.

## REFERENCES

- Alonso, R., et al. 2004, ApJ, 613, L153
- Brown, T.M. 2003, ApJ, 593, L125
- Bond, I.A. et al. 2004, ApJ, 606, L155
- Bouchy, F., Pont, F., Santos, N.C., Melo, C., Mayor, M., Queloz, D., & Udry, S. 2004, A&A, 421, L13-L16.
- Bouchy, F., Pont, F., Melo, C., Santos, N.C., Mayor, M., Queloz, D., & Udry, S. 2005, A&A, 431, 1105-1121.
- Burke, C.J., Gaudi, B.S., DePoy, D.L., & Pogge, R.W. 2005, AJ, submitted (astro-ph/0512207)
- Butler, R.P., et al. 2002, ApJ, 578, 565
- Cumming, A., Marcy, G.W., & Butler, R.P. 1999, ApJ, 526, 890
- Cumming, A. 2004, MNRAS, 354, 1165
- Dong, S. et al. 2005, ApJ, submitted (astro-ph/0507079)
- Drake, A.J. 2003, ApJ, 589, 1020-1026.
- Dreizler, S., Rauch, T., Hauschildt, P., Schuh, S.L., Kley, W., & Werner, K. 2002, A&A, 391, L17-L20.
- Duquennoy, A. & Mayor, M. 1991, A&A, 248, 485
- European Space Agency (ESA). 1997, The *Hipparcos* and Tycho Catalogues (SP-1200, Noordwijk: ESA)
- Fischer, D.A. et al. 2005, ApJ, 620, 481
- Fischer, D.A. & Valenti, J. 2005, ApJ, 622, 1102
- Gallardo, J., Minniti, D., Valls-Gabaud, D., & Rejkuba, M. 2005, A&A, 431, 707-720.
- Gaudi, B.S. & Sackett, P.D. 2000 ApJ, 528, 56

- Gaudi, B.S. et al. 2002, ApJ, 566, 463
- Gaudi, B.S. 2005, ApJ, 628, L73
- Gaudi, B.S., Seagar, S., & Mallen-Ornelas, G. 2005, ApJ, 623, 472
- Gilliland, R.L., et al. 2000, ApJ, 545, L47
- Gould, A. & Morgan, C.W. 2003, ApJ, 585, 1056.
- Heinze, A.N. & Hinz, Philip M., AJ, 130, 1929
- Hoekstra, H., Wu, Y., & Udalski, A. 2005, ApJ, 626, 1070
- Holman, M.J., Winn, J.N., Stanek, K.Z., Torres, G., Sasselov, D.D., Allen, R.L., & Fraser, W. 2005 ApJ, submitted (astro-ph/0506569)
- Konacki, M., Torres, G., Jha, S., & Sasselov, D.D. 2003a, Nature, 421, 507
- Konacki, M., Torres, G., Sasselov, D.D., & Jha, S. 2003, ApJ, 597, 1076-1091.
- Konacki, M. et al. 2004, ApJ, 609, L37-L40.
- Konacki, M., Torres, G., Sasselov, D.D., & Jha, S. 2005 ApJ, 624, 372-377.
- Kovács, G., Zucker, S., & Mazeh, T. 2002, A&A, 391, 369-377.
- Marcy, G.W., Butler, R.P., Vogt, S.S., Fischer, D.A., Henry, G.W., Laughlin, G., Wright, J.T., & Johnson, J.A. 2005, ApJ, 619, 570
- Mayor, M., Udry, S., Naef, D., Pepe, F., Queloz, D., Santos, N.C., & Burnet, M. 2004, A&A, 415, 391
- Mochejska, B.J., et al. 2005, AJ, 129, 2856
- Moutou, C., Pont, F., Bouchy, F., & Mayor, M. 2004, A&A, 424, L31
- Naef, D., Mayor, M., Beuzit, J.L., Perrier, C., Queloz, C., Sivan, J.P. & Udry, S. 2005 Cool Stars, Stellar Systems, and the Sun, 13th Cambridge Workshop, F. Favata, GAJ Hussain & B.Battrick, eds. (Noordwijk: ESA) (astro-ph/0409230)
- Nelson, A.F., & Angel, J.R.P. 1998, ApJ, 500, 940
- Pepper, J., Gould, A., & DePoy, D.L. 2003, Acta Astronomica, 53, 213-228.

- Pont, F., Bouchy, F., Queloz, D., Santos, N.C., Melo, C., Mayor, M., & Udry, S. 2004, *A&A*, 426, L15-L18.
- Pont, F. 2005, Status of and Prospects for Hot Jupiter Studies, L. Arnold, F. Bouchy, and C. Moutou, eds.
- Pont, F., Bouchy, F., Melo, C., Santos, N.C., Mayor, M., Queloz, D., & Udry, S. 2005, *A&A*, 438, 1123
- Santos, N.C., Israelian, G., & Mayor, M., 2004 *A&A*, 415, 1153
- Santos, N.C., Israelian, G., Mayor, M., Bento, J.P., Almeida, P.C., Sousa, S.G., & Ecuivillon, A. 2005, *A&A*, 437, 1127
- Sirko, E. & Paczyński, B. 2003, *ApJ*, 592, 1217-1224.
- Wolszczan, A., & Frail, D.A. 1992, *Nature*, 355, 145
- Udalski, A., Szewczyk, O., Zebrun, K., Pietrzynski, G., Szymanski, M., Kubiak, M., Soszynski, I., & Wyrzykowski, L. 2002a, *Acta Astron.*, 52, 317
- Udalski, A., Zebrun, K., Szymanski, M., Kubiak, M., Soszynski, I., Szewczyk, O., Wyrzykowski, L., & Pietrzynski, G. 2002, *Acta Astronomica*, 52, 115-128.
- Udalski, A., Szewczyk, O., Zebrun, K., Pietrzynski, G., Szymanski, M., Kubiak, M., Soszynski, I., & Wyrzykowski, L. 2002, *Acta Astronomica*, 52, 317-359.
- Udalski, A., et al. 2002, *Acta Astron.*, 52, 1
- Udalski, A., Pietrzynski, G., Szymanski, M., Kubiak, M., Zebrun, K., Soszynski, I., Szewczyk, O., & Wyrzykowski, L. 2003, *Acta Astronomica*, 53, 133-149.
- Udalski, A., Szymanski, M.K., Kubiak, M., Pietrzynski, G., Soszynski, I., Zebrun, K., Szewczyk, O., & Wyrzykowski, L. 2004, *Acta Astronomica*, 54, 313
- Udalski, A. et al. 2005, *ApJ*, 629 L49
- Weldrake, D.T.F., Sackett, P.D., Bridges, T.J., & Freeman, K.C. 2005, *ApJ*, 620, 1043

Table 1. Cuts in Data and Model

Number	Cut/Procedure	Data	Model
1.	Data Reduction	Yes	No
2.	Systematics Removal	Yes	No
3.	Saturation	Yes	Yes
4.	$\delta < 0.08$ mag	Yes	Yes
5.	$1.052 < (P/\text{day}) < 10$	Yes	Yes
6.	$\sigma < 0.015$ mag	Yes	Yes
7.	$\alpha > 9$	Yes?	Yes
8.	$SDE > \max[3, (4.9 - 0.1\alpha)]$	Yes	Yes?
9.	color-mag (bulge only)	Yes	Yes
10.	$> 3$ (or 2) Transits	Yes	Yes?
11.	$\delta < 0.04$ mag	Yes	Yes
12.	$P < 5$ days	Yes	Yes
13.	$\alpha > 11$	Yes?	Yes
14.	Period Recovery	Yes	Yes?
15.	By-eye Culling	Yes	Yes?
16.	Eclipsing Binaries	Yes	No
17.	Rapid Rotators	Yes	No
18.	$(V - I)_0 > 0.4$	Yes?	Yes
19.	$V < 17.5$	Yes?	Yes
20.	Unresolved Binaries	Yes	No



Table 2. Confirmed Transiting Planets

Name	Field	Period (days)	$I$	$\Delta I$	$N_{\text{tr}}$	$r/r_J$	$R_*/R_\odot$	$M/M_J$	$S/N$
OGLE-TR-10	bulge	3.1014	14.76	0.019	7	1.16	1.18	0.54	17.61
OGLE-TR-56	bulge	1.21193	15.25	0.013	12	1.23	1.10	0.9	17.88
OGLE-TR-111	Carina	4.01610	15.63	0.019	9	1.00	0.85	0.53	17.85
OGLE-TR-113	Carina	1.43250	14.50	0.030	10	1.09	0.78	1.35	39.49
OGLE-TR-132	Carina	1.68965	15.80	0.011	11	1.13	1.43	1.19	12.61

Note. — The mass and radius estimates for OGLE-TR-10 are from Holman et al. (2005), while those of OGLE-TR-132 are from Moutou et al. (2004). The S/N is derived from the original data using the Kovács et al. (2002) algorithm and eq. (1). The remaining data are from the papers in which the candidates were announced: (Udalski et al. 2002a,b,c, 2003); or confirmed as planets (Konacki et al. 2003a, 2005; Bouchy et al. 2004; Pont et al. 2004).

Table 3. Unclassified Candidates

Name	Field	Period (days)	$I$	$\Delta I$	$N_{\text{tr}}$
OGLE-TR-51	bulge	1.74812	16.71	0.034	5
OGLE-TR-134	bulge	4.53720	13.49	0.011	2
OGLE-TR-137	bulge	2.53782	15.85	0.030	7
OGLE-TR-82	Carina	0.76416	16.30	0.034	22

Table 4. Fraction of Stars Probed

$V_{\max}$	Carina			Bulge		
	$N_S$	$N_D$	$N_S/N_D$	$N_S$	$N_D$	$N_S/N_D$
15.5	930	8490	0.11	1057	7641	0.138
16.0	1766	12816	0.14	1634	13057	0.125
16.5	2969	18510	0.16	2309	23517	0.098
17.0	4486	27344	0.16	2909	42930	0.068
17.5	6153	39207	0.16	3287	79709	0.041
18.0	7542	54430	0.14	3397	156326	0.022
18.5	8382	74506	0.11	3414	278524	0.012

Note. —  $N_S$  is the number of stars around which a planet orbiting edge on with  $r = 1.2 r_J$  and  $a = 7.94 R_\odot$  could be detected, while  $N_D$  is the total number of stars in the field.

Table 5. Planet Frequency by Period

$P/\text{day}$	Carina		Bulge		Total		Frequency
	$N_p$	Planets	$N_p$	Planets	$N_p$	Planets	
1.0-2.0	885	2	495	1	1380	3	0.22%
2.0-3.0	456	0	226	0	682	0	
3.0-4.0	266	0	120	1	386	1	0.26%
4.0-5.0	163	1	69	0	232	1	0.43%

Note. — Values are averaged over planet radii ranging from  $1.00 r_J$  to  $1.25 r_J$ .

Table 6. Planet Frequency by Radius

$r/r_J$	Carina		Bulge		Total		Frequency
	$N_p$	Planets	$N_p$	Planets	$N_p$	Planets	
0.60	5	0	1	0	6	0	
0.65	10	0	4	0	14	0	
0.70	20	0	8	0	28	0	
0.75	35	0	15	0	50	0	
0.80	58	0	25	0	83	0	
0.85	91	0	39	0	130	0	
0.90	132	0	58	0	190	0	
0.95	184	0	83	0	267	0	
1.00	244	1	113	0	357	1	0.28%
1.05	314	0	150	0	464	0	
1.10	392	1	194	0	586	1	0.17%
1.15	477	1	244	1	721	2	0.28%
1.20	567	0	301	0	868	0	
1.25	661	0	363	1	1024	1	0.10%
1.30	759	0	432	0	1191	0	
1.35	856	0	503	0	1359	0	
1.40	952	0	577	0	1529	0	
1.45	1046	0	654	0	1700	0	
1.50	1136	0	731	0	1867	0	
1.55	1225	0	811	0	2036	0	
1.60	1312	0	893	0	2205	0	
1.65	1393	0	974	0	2367	0	
1.70	1467	0	1052	0	2519	0	

Note. — Values are averaged over periods from one to five days. See Fig. 11 for averages broken into two intervals:  $1 < P/\text{day} < 3$  and  $3 < P/\text{day} < 5$ .

Table 7. Fraction in Resonances

In Resonance	2 days	3 days	4 days	Total
Percent of Periods	1.3%	1.9%	2.6%	5.8%
Percent of Sensitivity	1.6%	2.5%	3.3%	7.4%

Table 8. Semimajor-Axis Power Laws

$\log(r/r_J)$	$\gamma (N_p = a^\gamma)$
–0.10	$-3.05 \pm 0.05$
–0.06	$-2.75 \pm 0.06$
–0.02	$-2.46 \pm 0.05$
0.02	$-2.23 \pm 0.04$
0.06	$-2.03 \pm 0.04$
0.10	$-1.86 \pm 0.03$

Note. — Pepper et al. (2003) predict  $N_p \propto a^\gamma$  with  $\gamma = -5/2$  for transit surveys of nearby stars

Table 9. Planet-Radius Power Laws

$\log(a/R_\odot)$	$\gamma (N_p = r^\gamma)$
0.60	$4.5 \pm 0.3$
0.68	$4.9 \pm 0.3$
0.76	$5.4 \pm 0.4$
0.84	$5.9 \pm 0.4$
0.92	$6.4 \pm 0.4$
1.00	$6.9 \pm 0.4$

Note. — Pepper et al. (2003) predict  $N_p \propto r^\gamma$  with  $\gamma = 6$  for transit surveys of nearby stars.

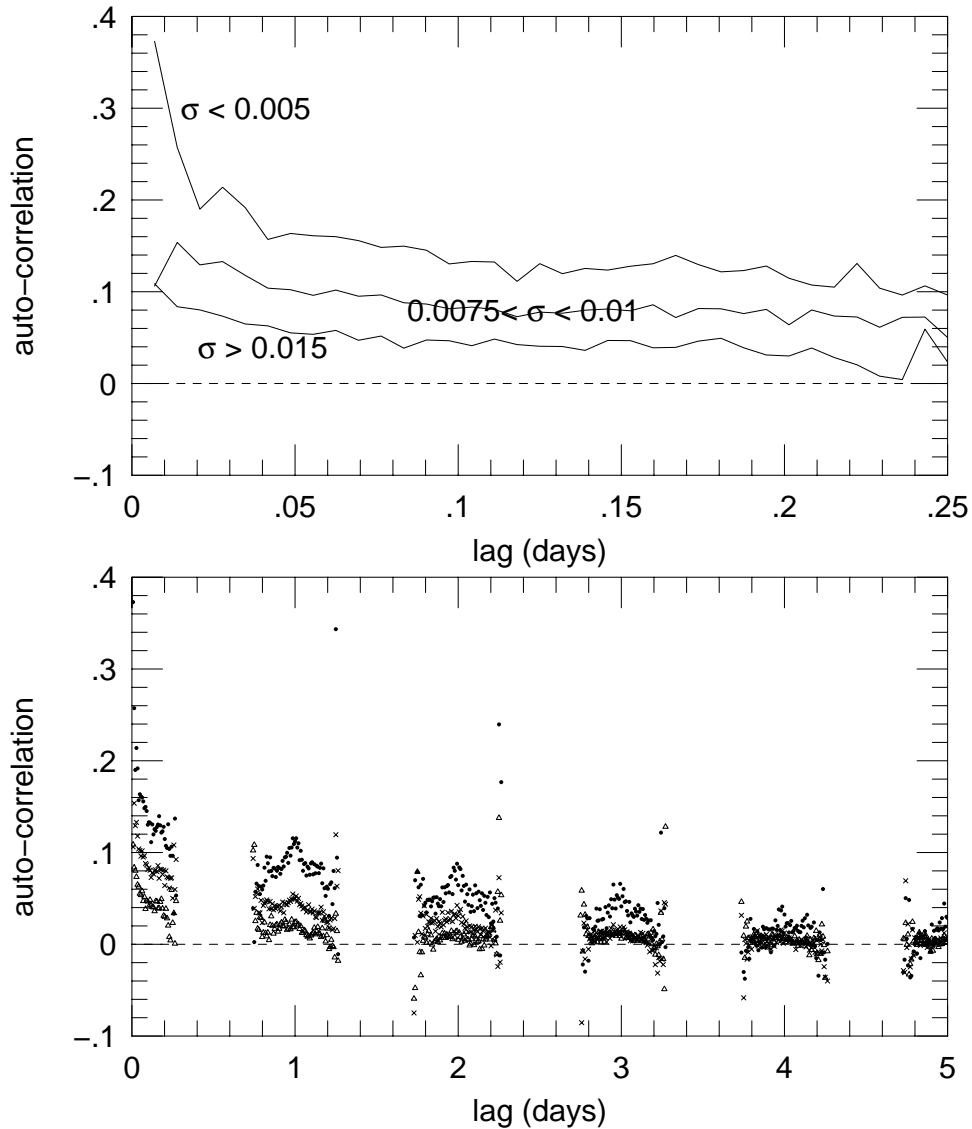


Fig. 1.— Autocorrelation function for transit data toward OGLE subfield Car100.1. The upper panel shows lag times ranging from 10 minutes to 6 hours for three subsamples of the data with photometric errors (determined from the scatter) in the three indicated ranges. The lower panel shows data for these same subsamples over 5 days. For lags similar to a transit duration (few hours) the autocorrelation is significant, particularly at bright magnitudes (small errors), which could in principle affect the detectability of the transits.

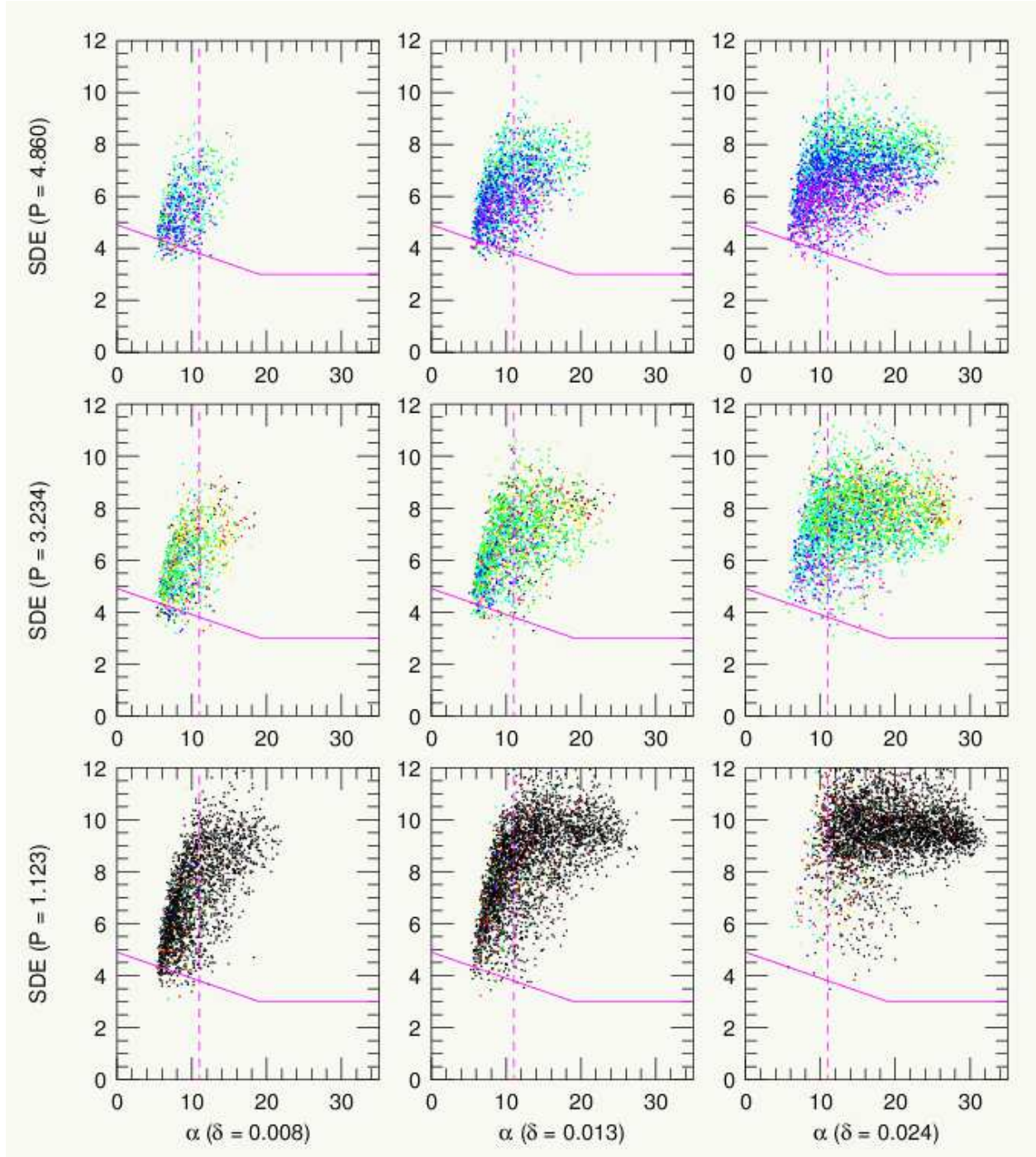


Fig. 2.— Signal detection efficiency ( $SDE$ , measuring the strength of the detection relative to the noise in the periodogram power spectrum) vs. the signal-to-noise ratio parameter  $\alpha = [(S/N)^{-2} + N_{\text{obs}}^{-1}]^{-1/2}$ . The nine panels show Monte Carlo simulations in which transits are injected into the data stream of each of the  $\sim 4000$  stars monitored in the OGLE-III Carina subfield Car100.1. The period  $P$  and transit depth  $\delta$  are held fixed at the indicated values, while the phase and inclination of the transit are drawn randomly. The selection criteria for  $\alpha$  and  $SDE$  are shown by magenta lines. Essentially all simulated light curves that survive the  $\alpha > 11$  cut also satisfy the  $SDE$  cut, which means that it is not necessary to model the  $SDE$ . The points are color coded according to the number of distinct transits



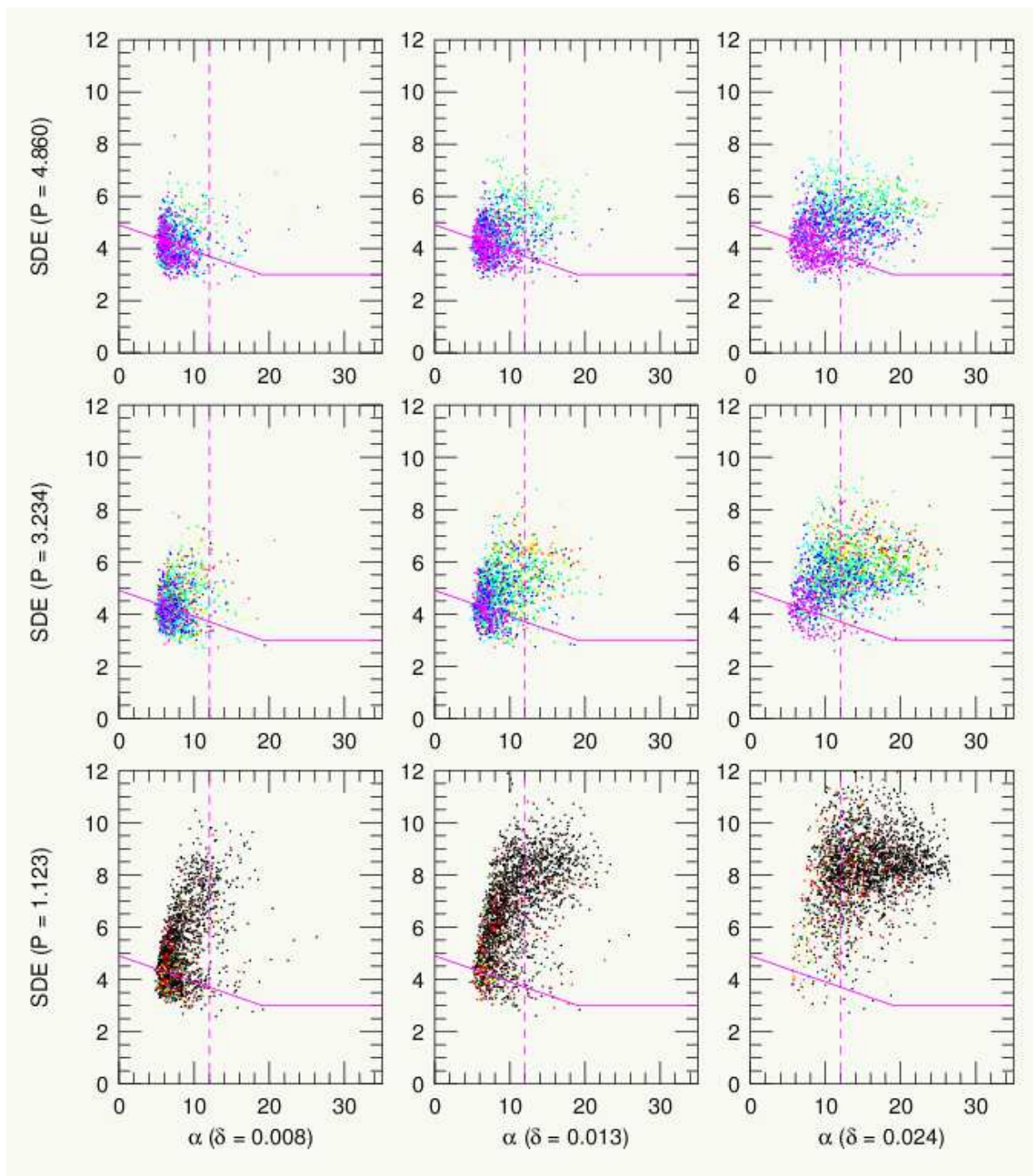


Fig. 3.— Similar to Fig. 2 but for OGLE-III bulge subfield BLG100.1. For shorter periods  $P \lesssim 3$  days, transit candidates that survive the  $\alpha$  cut also pass the  $SDE$  cut (as was true toward Carina). However, at the longest periods,  $P \sim 5$  days, about 10% of transits with  $\alpha > 11$  fail the  $SDE$  cut, a loss that must be taken into account when determining planetary frequency.

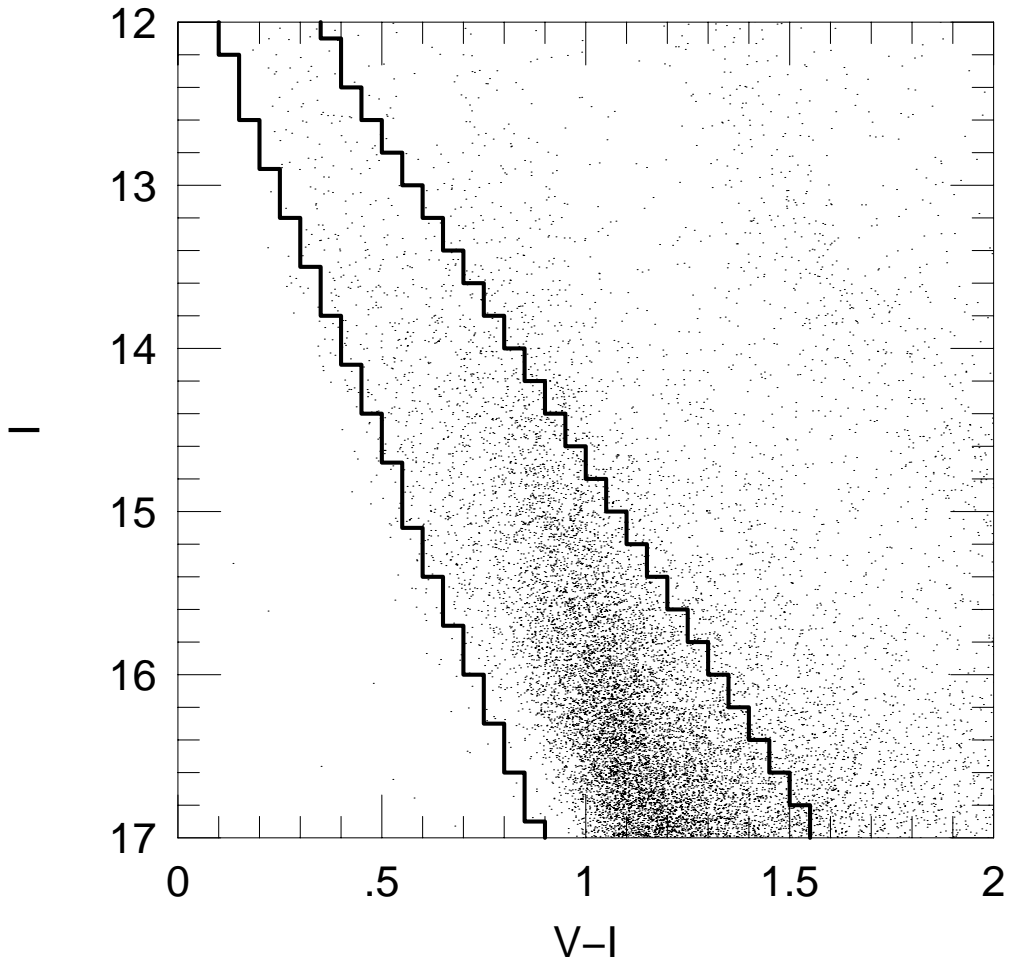


Fig. 4.— OGLE-II Carina CMD. The region inside the bold histograms is used to fit a stellar model used along the OGLE-III Carina line of sight.

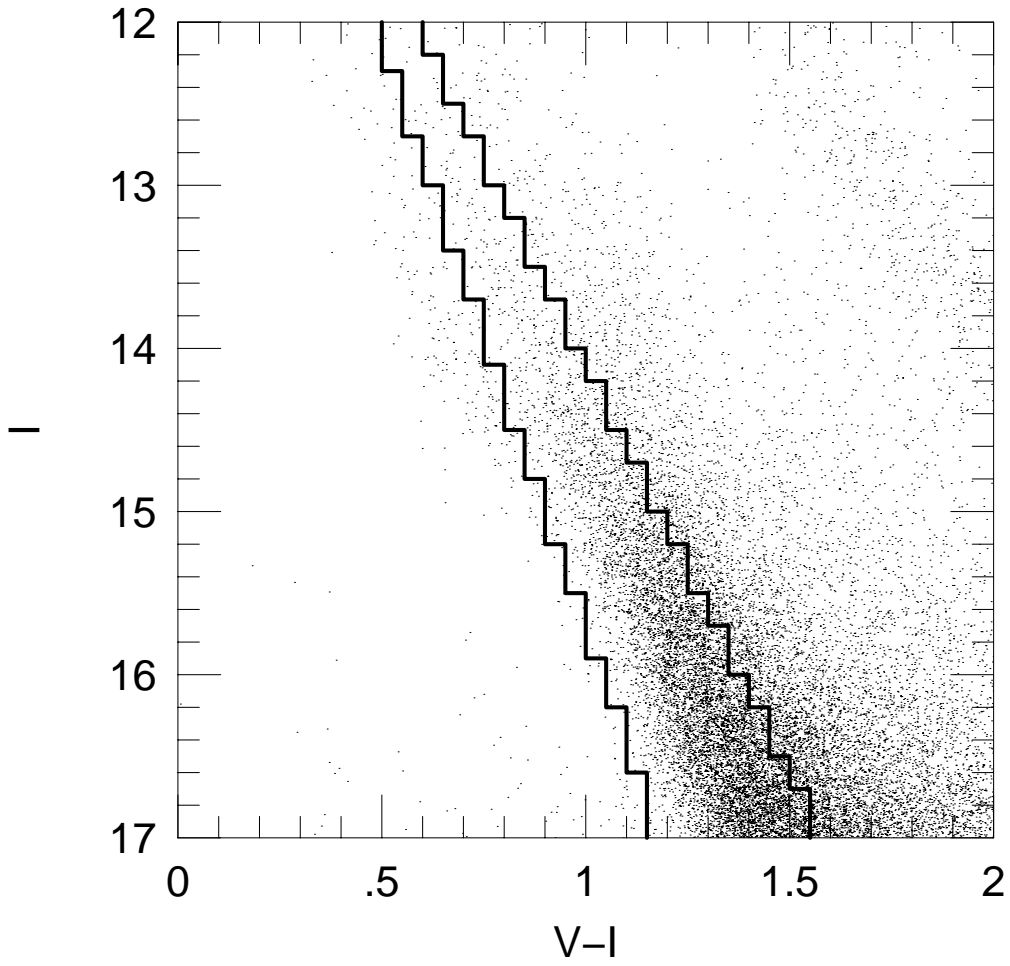


Fig. 5.— OGLE-II bulge CMD. The region inside the bold histograms is used to fit a stellar model used along the OGLE-III bulge line of sight.

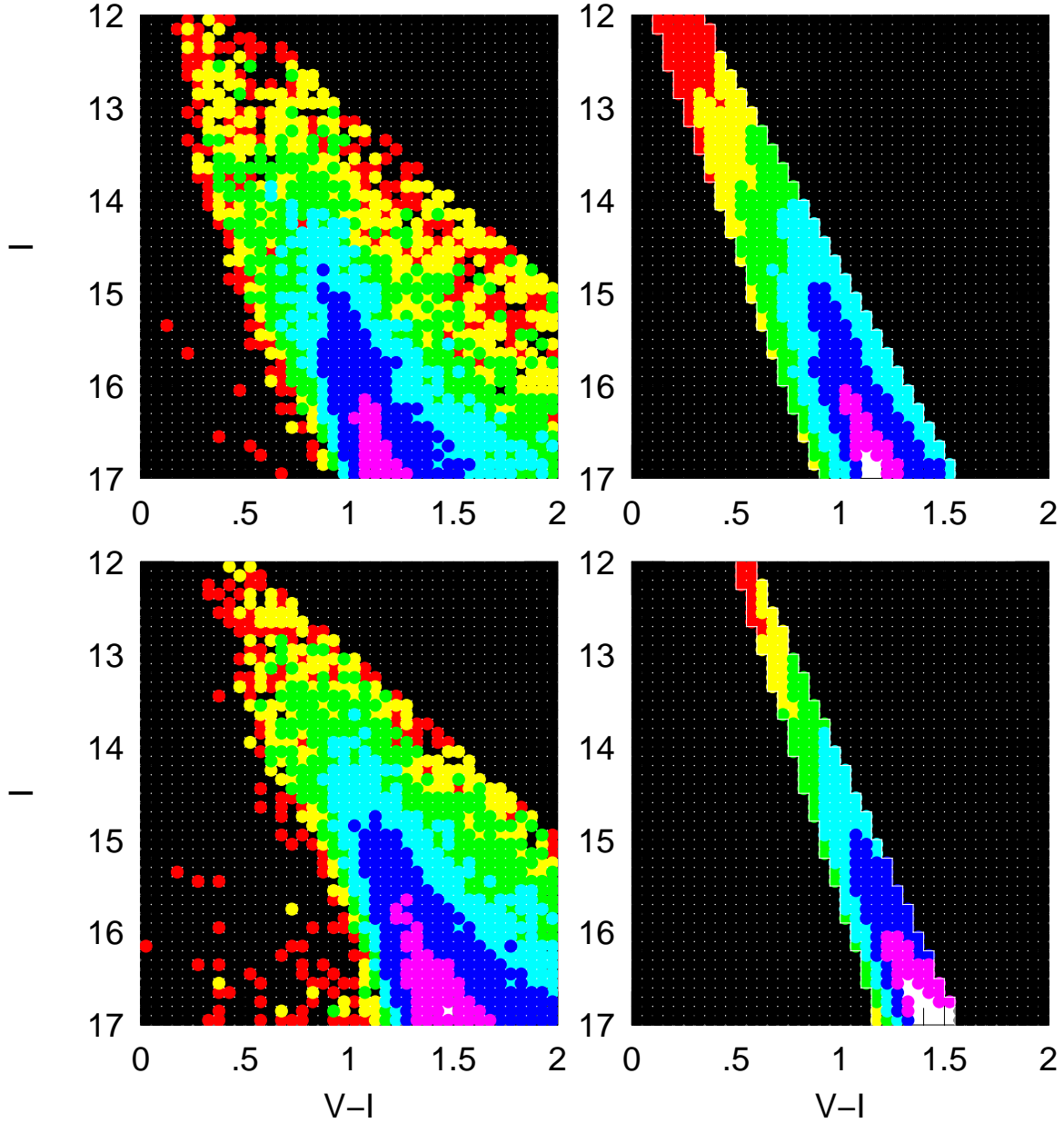


Fig. 6.— Observed (left) and predicted (right) CMD stellar densities  $\rho$  for Carina (top) and the bulge (bottom). Contour levels in stars per  $(0.05 \times 0.1)$  bin are  $\rho < 0.02$ , 1, 3, 9, 27, 81, 140 for black, red, yellow, green, cyan, blue, magenta, and  $\rho > 140$  for white. For Carina, the predictions are based on the best fit model with parameters  $(dA_I/dD)_0 = 0.174 \text{ kpc}^{-1}$ ,  $R_{VI} = 2.23$ ,  $h_{\text{dust}} = 273 \text{ pc}$ , and  $K = 0.81$ , while for the bulge these parameters are  $(dA_I/dD)_0 = 0.435 \text{ kpc}^{-1}$ ,  $R_{VI} = 2.56$ ,  $h_{\text{dust}} = 65 \text{ pc}$ , and  $K = 1.08$ .

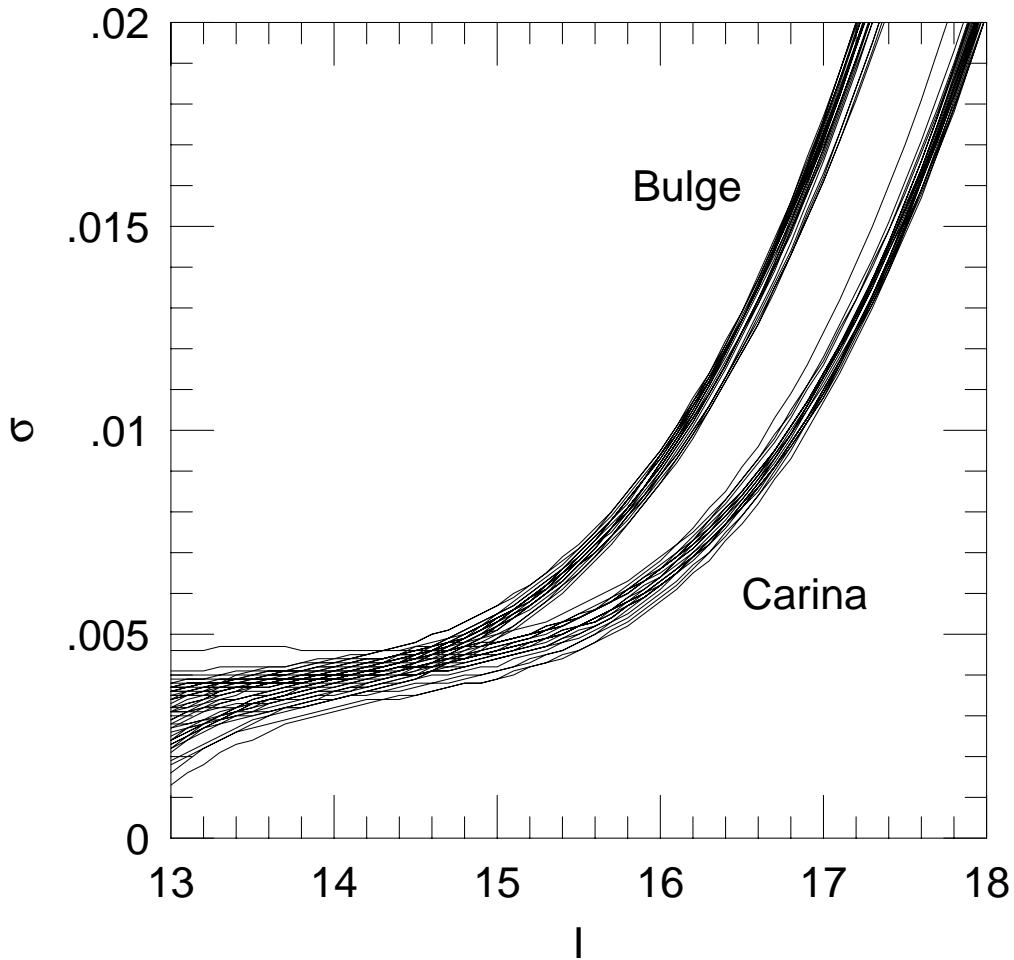


Fig. 7.— Error functions vs.  $I$  magnitude for each of 48 subfields, 8 for each of three fields in each of two target directions (Carina and bulge). Each is a cubic that is fit to the data after recursive elimination of  $2.5\sigma$  outliers. The 24 error functions in each direction are tightly clustered. The bulge errors are worse at faint magnitudes because of shorter exposures and higher background.

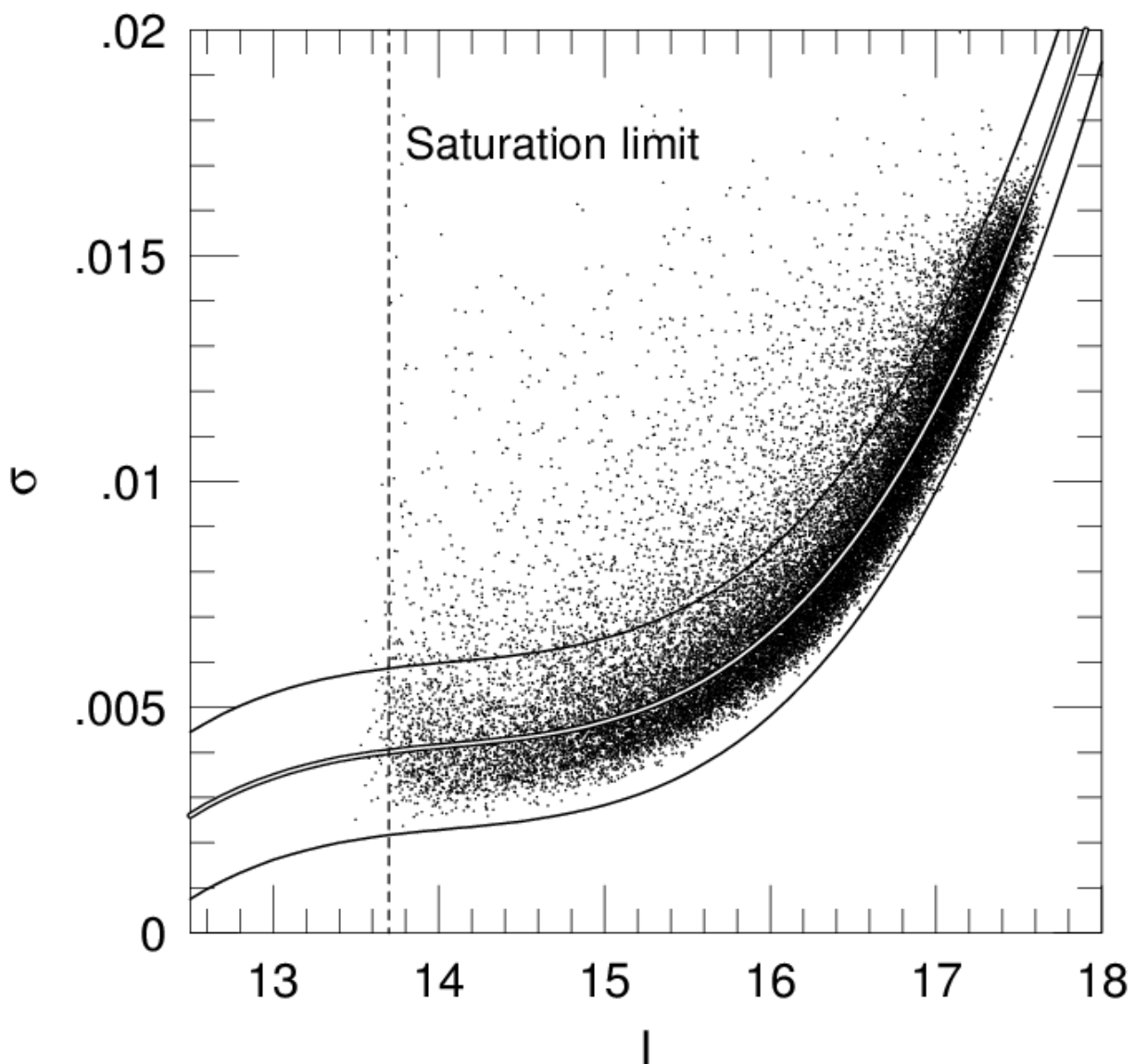


Fig. 8.— Mean error function (*silhouette curve*) vs.  $I$  magnitude for Carina. Points are the errors (determined from the scatter) of individual stars in CAR100, the only one of the three Carina fields that can be directly calibrated. The *solid curves* indicate the  $2.5\sigma$  limits beyond which data points were removed from the fit. The 10% of stars so eliminated are assumed to contribute to planet detection with half the efficiency of the 90% that are well represented by the mean error function. The dashed vertical line represents the saturation threshold, which is identified from the points in this diagram to be at  $I = 13.7$ .

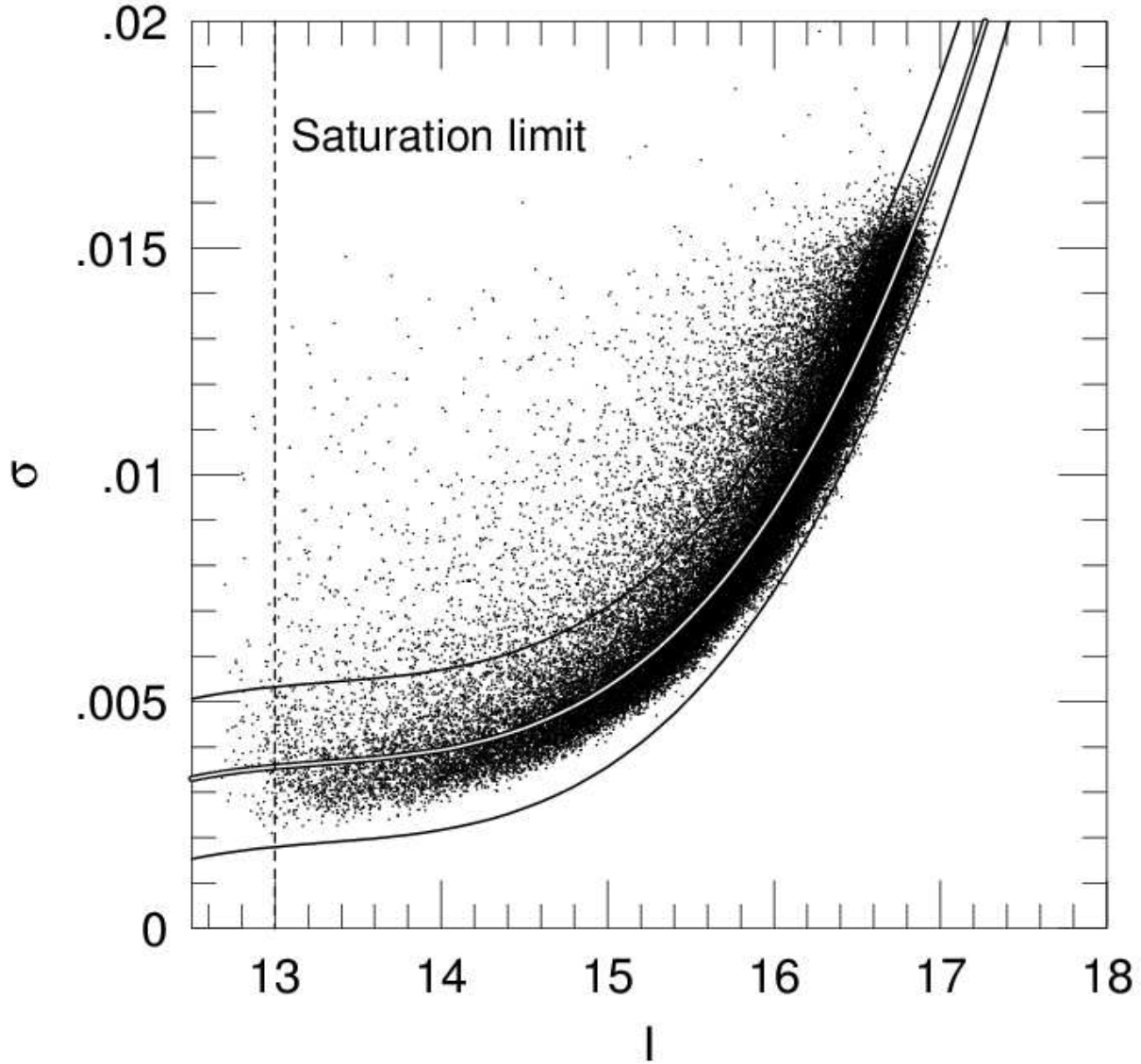


Fig. 9.— Mean error function (*silhouette curve*) vs.  $I$  magnitude for the bulge. Similar to Fig. 8 except that in this case all three bulge fields are included in the fit. Again, roughly 10% of the stars are eliminated from the fit by the  $2.5\sigma$  criterion (*solid curves*). The dashed vertical line represents the saturation threshold, which is identified from the points in this diagram to be at  $I = 13.0$ .

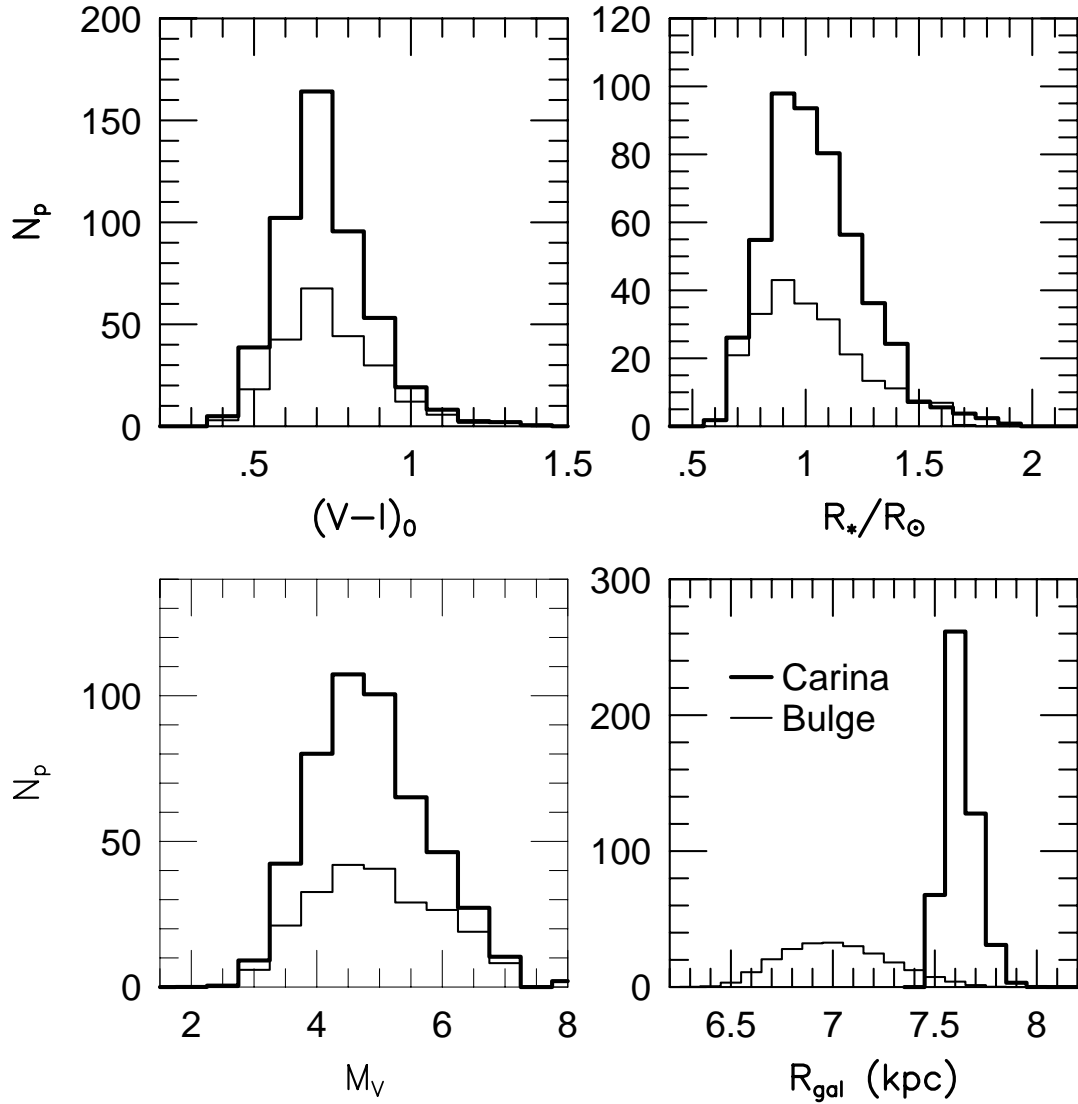


Fig. 10.— Distributions of four properties of the stellar populations probed for planets of radius  $r = 1.2 r_J$  and  $a = 7.94 R_\odot$  toward the Carina (*bold histograms*) and bulge (*solid histograms*) fields. Shown are the dereddened  $(V - I)_0$  colors, the stellar radii  $R_*$ , the absolute magnitudes  $M_V$ , and the Galactocentric distance  $R_{\text{gal}}$ . The Galactic-model parameters are  $(dA_I/dI)_0 = 0.174 \text{ kpc}^{-1}$ ,  $R_{VI} = 2.23$ ,  $h_{\text{dust}} = 273 \text{ pc}$ , and  $K = 0.81$  for Carina and  $(dA_I/dI)_0 = 0.435 \text{ kpc}^{-1}$ ,  $R_{VI} = 2.56$ ,  $h_{\text{dust}} = 65 \text{ pc}$ , and  $K = 1.08$  for the bulge.



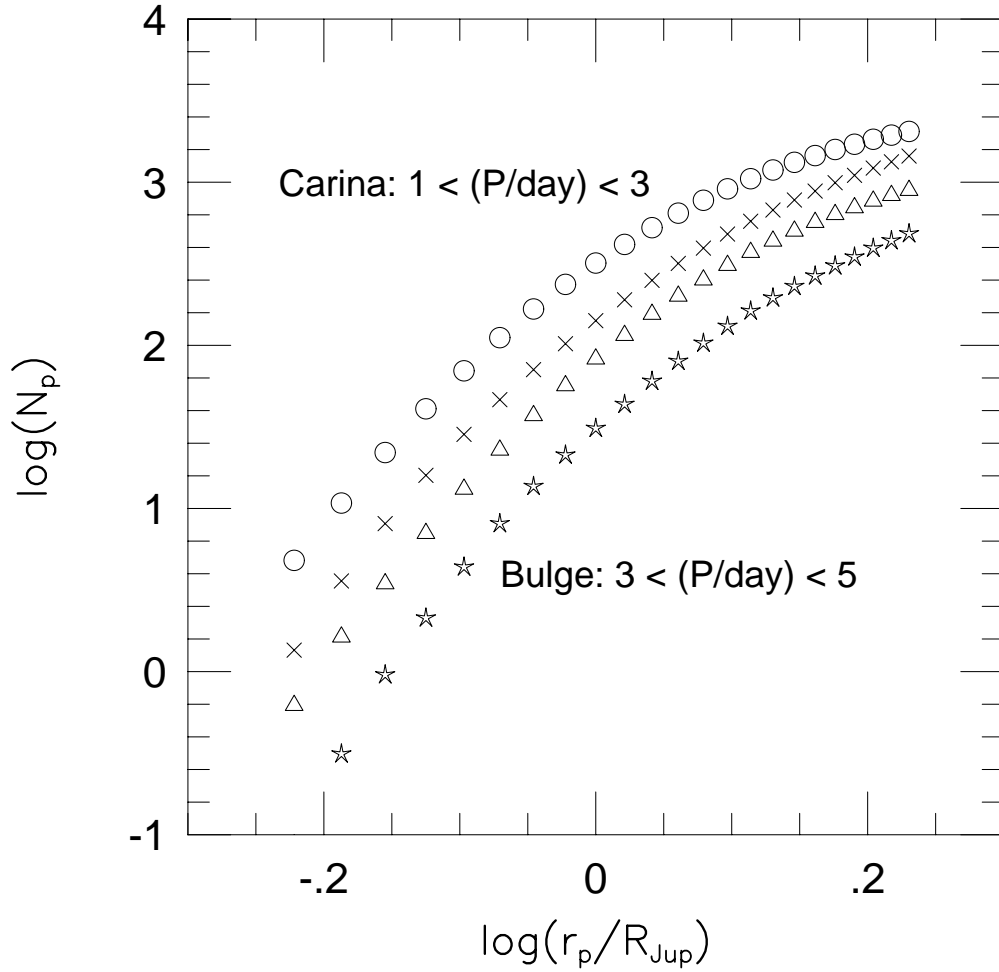


Fig. 11.— Number of systems probed ( $N_p$ ) as a function of radius averaged over a range of periods. Carina:  $1 < (P/\text{day}) < 3$  (circles),  $3 < (P/\text{day}) < 5$  (triangles). Bulge:  $1 < (P/\text{day}) < 3$  (crosses),  $3 < (P/\text{day}) < 5$  (stars).

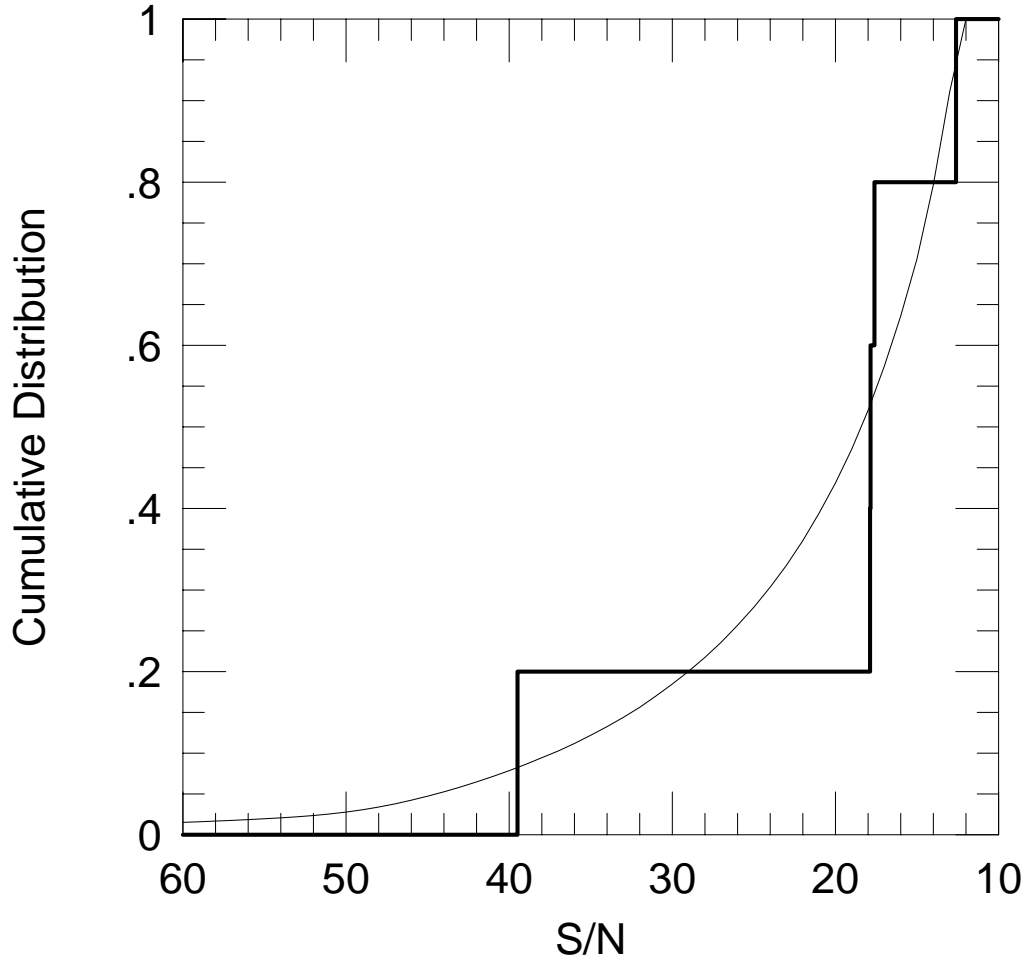


Fig. 12.— Cumulative distribution as a function of  $S/N$  of the 5 confirmed OGLE transiting planets (*bold histogram*) compared to the distribution expected from our model (*solid curve*). A KS test shows the the two are consistent at  $P(d = 0.342) = 0.50$ .

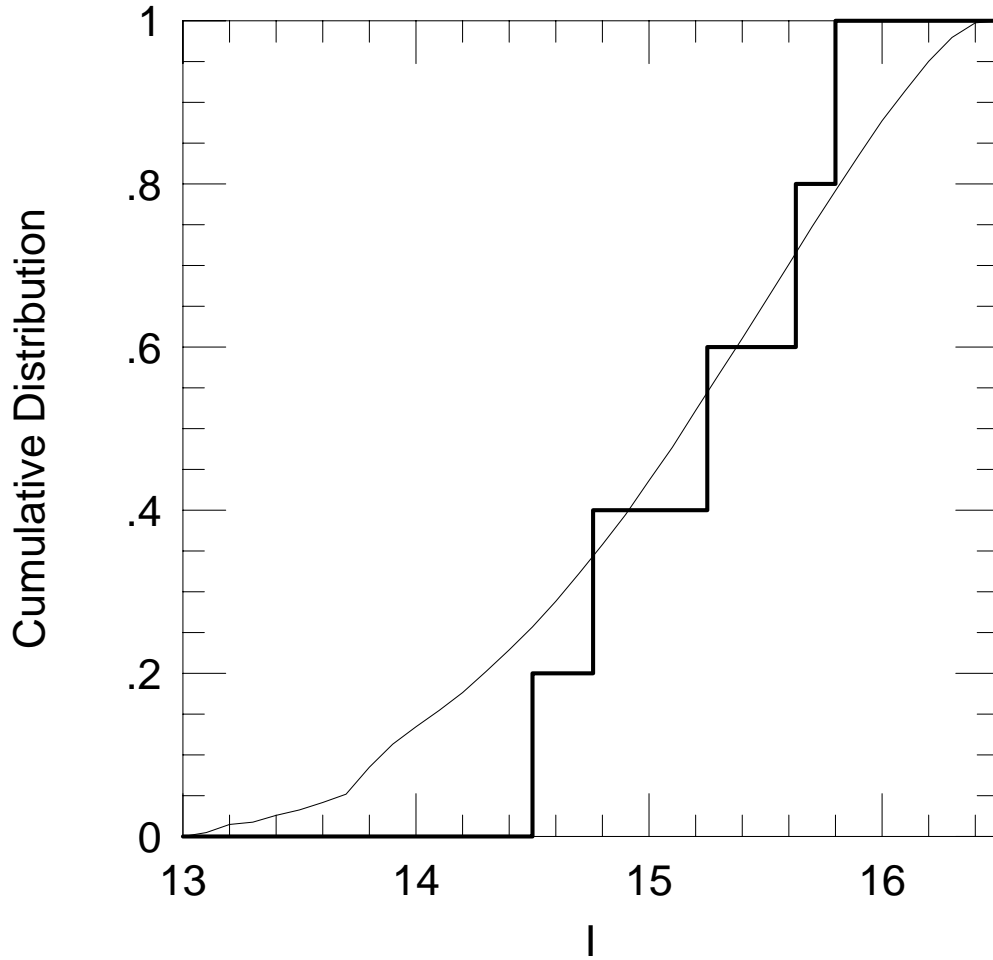


Fig. 13.— Cumulative distribution as a function of  $I$ -band apparent magnitude of the 5 confirmed OGLE transiting planets (*bold histogram*) compared to the distribution expected from our model (*solid curve*). A KS test shows the the two are consistent at  $P(d = 0.257) = 0.82$ .

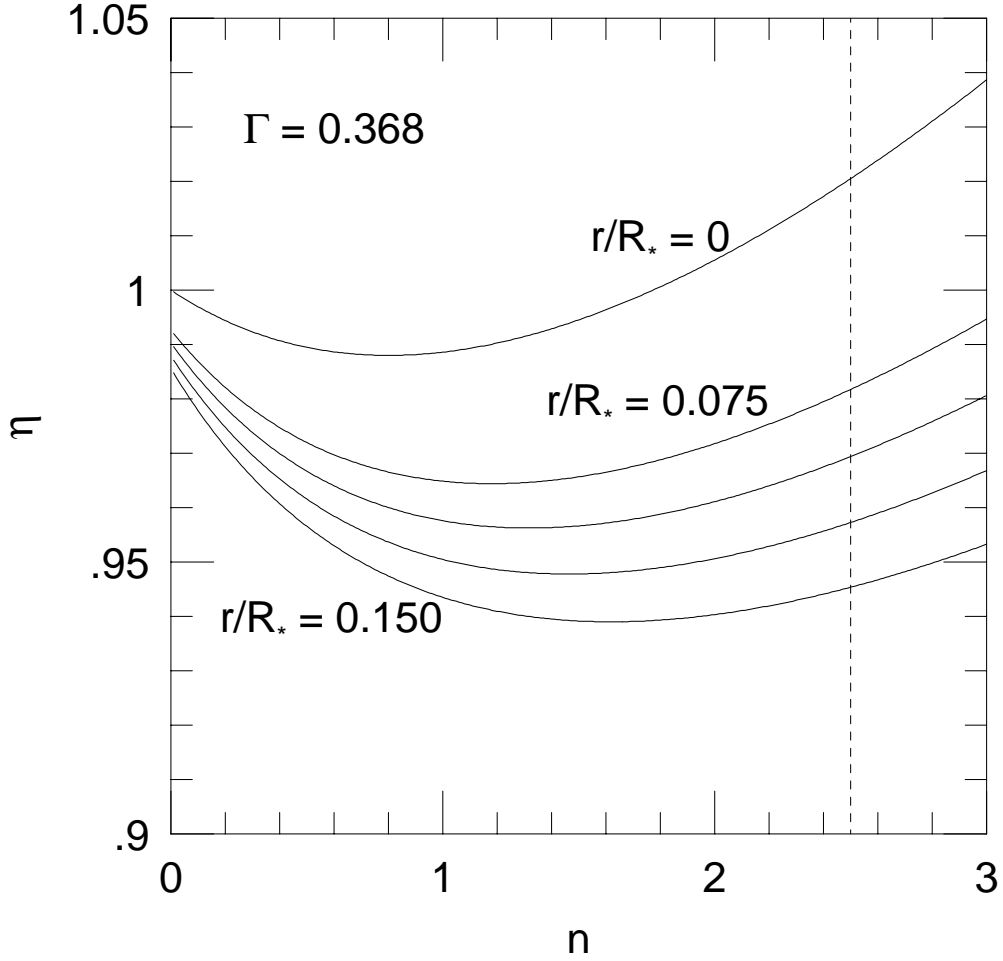


Fig. 14.— Combined effect of limb darkening and ingress/egress on the number of systems probed for planets relative to the case of a point-planet occulting a star of uniform surface brightness. The five curves show the degradation factor  $\eta$  as a function of power-law index  $n$ , for planet-star  $r/R_* = 0, 0.075, 0.1, 0.125$  and  $0.15$ . The power-law index parameterizes the growth of survey sensitivity as a function of  $S/N$  threshold, i.e.  $\propto (S/N)_{\min}^{-n}$ . The dashed line indicates  $n = 2.5$ , the value that most closely represents the behavior of the present survey.

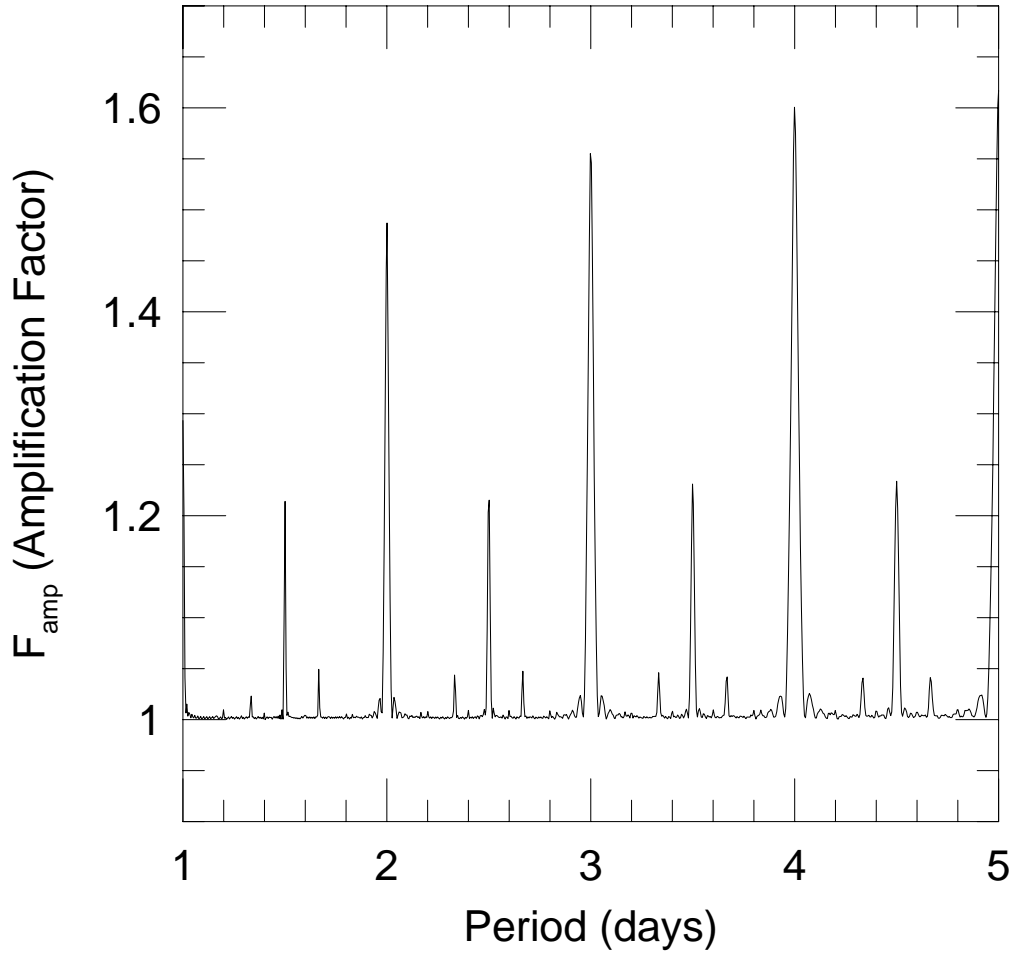


Fig. 15.— Period versus amplification factor  $F_{amp}$  for a 24-hour day, 6-hour night, 10-minute observations, an 80-day campaign, and a fraction  $f = 1/30(P/4 \text{ days})^{-2/3}$  of the orbit spent in transit.

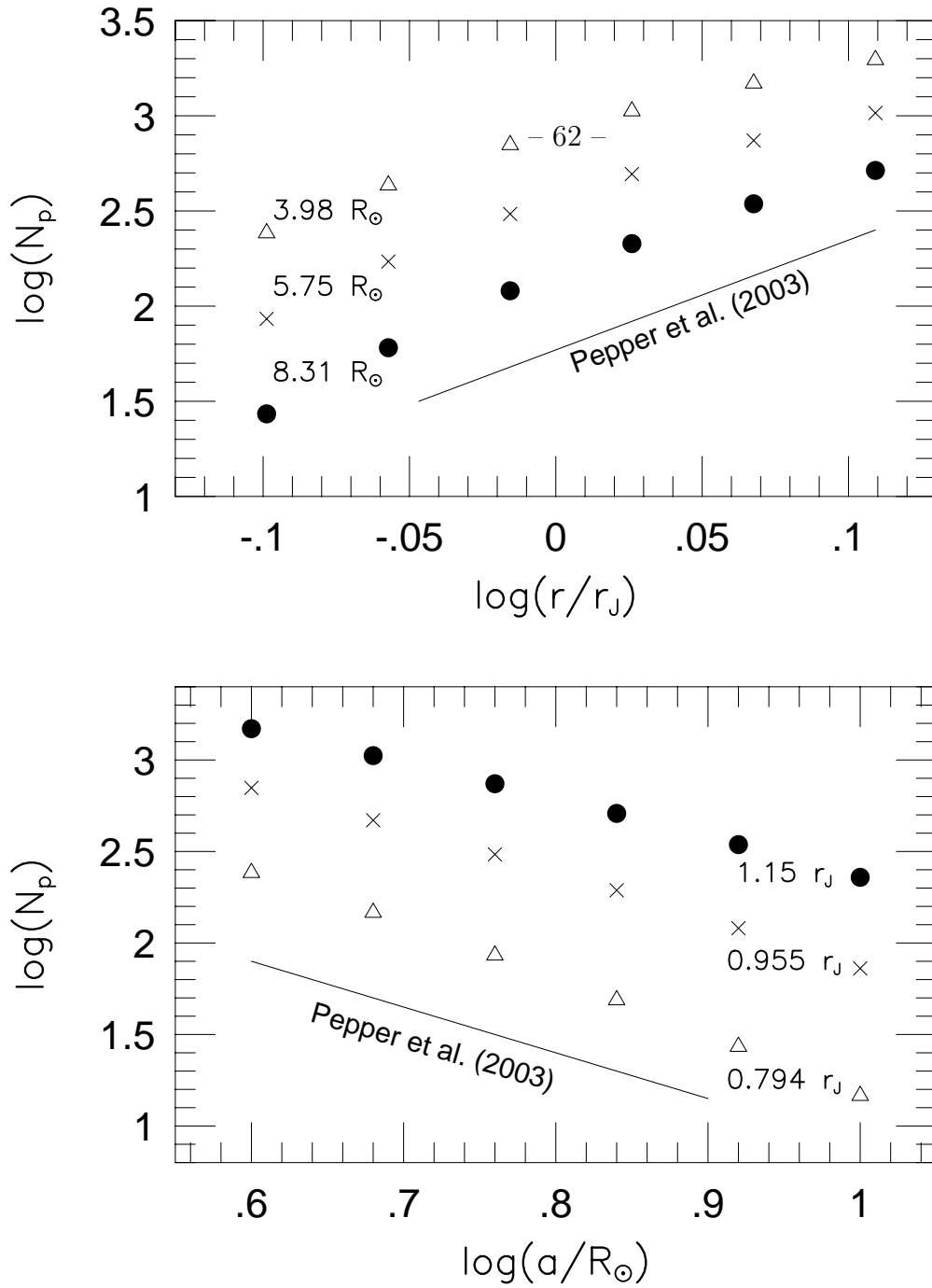


Fig. 16.— The top panel shows the number of systems probed for planets ( $N_p$ ) in the OGLE-III survey toward Carina as a function of the planet radius,  $r$ , for three values of the orbital semi-major axis,  $a = 3.98 R_\odot$  (triangles),  $a = 5.75 R_\odot$  (crosses), and  $a = 8.31 R_\odot$  (circles). The lower panel shows  $N_p$  as a function of  $a$  for three different values of the planet radius,  $r = 0.794 r_J$  (triangles),  $r = 0.955 r_J$  (crosses), and  $r = 1.15 r_J$  (circles). The solid lines in each panel represent the slopes of the scaling relations predicted by Pepper et al. (2003),  $N_p \propto a^{-5/2}$  and  $N_p \propto r^6$ , respectively.